Since January 2020 Elsevier has created a COVID-19 resource centre with free information in English and Mandarin on the novel coronavirus COVID-19. The COVID-19 resource centre is hosted on Elsevier Connect, the company's public news and information website.

Impact of natural ventilation on exposure to SARS-CoV 2 in indoor/semi-indoor terraces using CO_2 concentrations as a proxy

Esther Rivas [*], Jose Luis Santiago, Fernando Martín, Alberto Martilli

Atmospheric Pollution Division - Environmental Department Research Center for Energy, Environment, and Technology – CIEMAT, Avda. Complutense, 40, 28 040, Madrid, Spain

ARTICLE INFO

ABSTRACT

Nowadays, it is necessary a better airborne transmission understanding of respiratory diseases in shared indoor and semi-indoor environments with natural ventilation in order to adopt effective people's health protection measures. The aim of this work is to evaluate the relative exposure to SARS-CoV 2 in a set of virtual scenarios representing enclosed and semi-enclosed terraces under different outdoor meteorological conditions. For this purpose, indoor CO_2 concentration is used as a proxy for the risk assessment. Airflow and people exhaled CO_2 in different scenarios are simulated through Computational Fluid Dynamics (CFD) modelling with Unsteady Reynolds-Averaged Navier-Stokes (URANS) approach. Both spatial average concentrations and local concentrations are analyzed. In general, spatial average concentrations decrease as ventilation increases, however, depending on the people arrangement inside the terrace, spatial average concentrations and local concentrations can be very different. Therefore, for assessing the relative exposure to SARS-CoV 2 it is necessary to consider the indoor flow patterns between infectors and susceptibles. This research provides detailed information about CO_2 dispersion in enclosed/semi-enclosed scenarios, which can be very useful for reducing the transmission risk through better natural ventilation designs and improving the classic risk models since it allows to check their hypotheses in real-world scenarios. Although CFD ventilation studies in indoor/semi-indoor environments have been already addressed in the literature, this research is focused on restaurant terraces, scenarios scarcely investigated. Likewise, one of the novelties of this study is to take into account the outdoor meteorological conditions to appropriately simulate natural ventilation.

1. Introduction

Bioaerosols are solid or liquid particles whose size ranges from 0.1 μm to 100 μm, containing smaller particles of biological origin [1]. When people breathe, cough or sneeze, they emit bioaerosols to the air that can contain pathogens. Depending on their size, they can deposit quickly on surfaces because of the gravity effect (heavier bioaerosols) or remain suspended in the air (lighter bioaerosols) during hours [2] according to the ventilation-induced effects [3]. It can generate cross-infections and in fact, bioaerosols play an essential role in the transmission of respiratory diseases, such as tuberculosis and measles [4], influenza [5], SARS-CoV 1 [6] or MERS [7]. Today, it is well known by the scientific community this fact is also applicable to SARS-CoV 2 [8,9] and it has been already recognized by international organizations like WHO (World Health Organization) and CDC (Center for Disease Control and Prevention).

Europeans spend, on average, between 85% and 90% of their daily time in closed spaces or indoor environments according to a report published by the EC [10]. The risk of contagion of airborne diseases in these environments is greater than in open spaces or outdoor environments [11]. Therefore, it is usually recommended that some human activities would be carried out outdoor to reduce exposure to SARS-CoV 2 [12]. Depending on the country and the age, people spend different time eating and drinking in restaurants, cafes, and canteens [10]. This activity is usually carried out in shared indoor/semi-indoor environments and it could potentially represent high exposure to SARS-CoV 2 depending on the crowding and noising levels (bioaerosol emission increases with voice loudness [13], occupation times, venting and people face covering [14]).

Natural ventilation dilutes and removes the indoor bioaerosols by providing fresh air. For this reason, improving the natural ventilation (i.e. increasing the air renewal rate) in indoor/semi-indoor environments, like restaurants, cafes and canteens are recommended as a risk reduction measure [15]. But, depending on the flow patterns between people, the ventilation process (by providing high renewal rates) may decrease the cross-infection risk or it may increase the spread of diseases in shared environments. That is why, presently, more and more works highlight the importance of achieving adequate indoor air circulations to reduce airborne transmission [16–18]. Although most of these works are focused on indoor environments with mechanical ventilation [19], for example, inside hospitals [20–23].

To analyze natural ventilation in indoor/semi-indoor environments, both experimental and theoretical techniques can be used. A useful experimental technique is the Particle Image Velocimetry, PIV [24]. Nevertheless, in some cases, obtaining a complete information is techno-economically unfeasible from the experimental point of view. Theoretical techniques require using models able to simulate bioaerosols behavior in real scenarios. The classic Wells–Riley model [25] is commonly used to calculate the probability of infection from airborne diseases indoors, such as SARS-CoV 2. It depends on the quanta (viruses released), people exposure time, room ventilation flow rate, room volume, and other factors [26]. And one of their main hypotheses is that the quanta is completely mixed into the room. But in real real-world scenarios, this hypothesis hardly ever is verified. That is why the new versions of Wells–Riley model tries to overcome this limitation including a mixing factor [27]. This research gap is being covered by Computational Fluid Dynamics (CFD) models which are a very useful tool because provides detailed spatial information about the airflow and viruses concentrations (if sources are well characterized) in real indoor environments [28].

After the COVID19 pandemic lockdown, several activities were moved to the outdoor, for example, restaurants and bars closed their indoor stores but opened or extended their terraces even in wintertime. To shield the customers from the weather, their settings were outfitted with non-permanent or semi-permanent structures with light walls and roofs giving rise, in some cases, to almost indoor or semi-indoor terraces, which would not be able to comply with adequate ventilation [29].

The application of CFD models to study the exposure to SARS-CoV 2 in several real environments during COVID19 pandemic has been already addressed in the recent literature: in a grocery store [30], in a restaurant [31] or in a waiting room [32]. In addition, the local risk level has been analyzed in a classroom [33] or in a theater hall [34]. However, in these studies, natural ventilation has not been considered or not accurately considered despite being indoor/semi-indoor environments. For example [31], have simulated a restaurant with both mechanical and natural ventilation using constant and homogeneous boundary conditions. But natural ventilation, and consequently indoor airflow and bioaerosol dispersion, depend on the outdoor meteorological conditions (wind speed, direction, temperature, etc.), and not all of them are equivalent to indoor ventilation. Therefore, to fill this research gap, the domain of CFD simulations should cover not only indoor/semi-indoor environment, but also the nearby outdoor, in order to appropriately simulate the natural ventilation and its influence on indoor airflow and bioaerosol dispersion. The dependency of natural ventilation on the outdoor meteorological conditions is due to its driving forces are wind pressure, stack pressure (buoyancy), or a combination of both. And in all cases, the influence of outdoor conditions cannot be neglected. In the first case, the wind flow is induced by a pressure gradient between windward and leeward (different pressure coefficients). In the second case, the wind flow is induced by a temperature gradient between indoor and outdoor. And finally, in the third case, the wind flow is induced by a combination of both phenomena.

[35] studied wind speed effect on social distancing, but not the wind direction effect. And, for instance, the indoor flow patterns in a restaurant terrace are different depending on the wind direction and the design of the terrace (some of them have usually outfitted their setting with doors, windows, walls, and roofs). At the same time, the indoor bioaerosol concentrations in a restaurant terrace are different depending on indoor flow patterns and people arrangement inside the terrace.

Indoor CO_2 concentrations are commonly used as a proxy of the risk of respiratory diseases transmission [36–39] due to:

● these diseases are acquired mainly by inhaling infectious bioaerosols
● infectious bioaerosols are released to ambient air through the people exhaled air
● the people exhaled air CO_2 concentration is much higher than outdoor CO_2 concentration
● in indoor environments the main sources of CO_2 emissions are people.

But, depending on the bioaerosols size and the ventilation system, the dispersion of bioaerosols and CO_2 can be different [40]. numerically investigated the behavior of a gas tracer versus particles whose size ranges between 0.1 μm and 20 μm under three ventilation strategies: mixing ventilation (MV), displacement ventilation (DV), and under-floor air distribution (UFAD). They stated the movements of submicron particles are like tracer gases, whereas the gravitational effect should be taken into account for particles larger than 2.5 μm [41]. obtained similar conclusions using an Eulerian CFD model validated with particles whose size ranges between 0.5 μm and 1 μm and between 5 μm and 10 μm. Recently, [42]; carried out experimental work in a concert hall using an aerosol distribution whose size ranges from 0.1 μm to 10 μm with a peak in 0.3 μm (typical distribution for people during breathing) and a vertical ventilation system which provides fresh air from bottom to top. In this work, a good correlation between indoor aerosol and

CO_2 concentrations was found. In this context, this research is focused on small bioaerosols (order of 1 μm or lower), using CO_2 as a proxy, since:

● the exhaled bioaerosols size when people are talking ranges from 0.05 μm to 10 μm with the mean value of about 1 μm [13])
● the impact on health of these bioaerosols because, in addition to ultrafine particles, inhaled bioaerosols between 1 μm and 5 μm can go through the upper respiratory tract and have a high probability of deposition on the bronchial tree and alveoli [43].

Nowadays the dose of viable SARS-CoV 2 required to cause infection in another person is not well known, therefore, the problem needs to be addressed in relative terms, comparing different scenarios/situations.

Under this framework, the main objective of this study is to estimate the impact of natural ventilation on the relative exposure to SARS-CoV 2, using indoor CO_2 concentrations as a proxy, in a set of virtual indoor/semi-indoor scenarios representing multiple terrace configurations as a function of outdoor wind direction. For this purpose, CFD modelling is used with a URANS type turbulence approach which reproduces the real indoor flow patterns and several passive scalars transport equations to simulate people exhaled CO_2 concentrations. Therefore, one of the main novelties of this study is to take into account the outdoor meteorological conditions to appropriately simulate natural ventilation and its effects on indoor airflow and CO_2 dispersion considering a numerical domain that covers not only the terrace but also the nearby outdoor. In addition, the terraces investigated in the present study is an environment scarcely studied.

The goal of a good venting configuration is to ensure that most exhaled bioaerosols by the people are diluted and removed before being inhaled by the surrounding people. Therefore, the numerical results have been analyzed from both spatial average concentrations and a local concentrations point of view. Here, the relationship between flow patterns and indoor CO_2 concentrations for a wide range of scenarios is shown and the relative exposure to SARS-CoV 2 is studied assuming the same exposure time for all cases. These results can help to better understanding SARS-CoV 2 transmission in shared indoor and semi-indoor environments with natural ventilation and the used methodology can be useful to improve the risk classic models and to evaluate natural ventilation based strategies.

The work outline is the following: firstly, the material and method are described (CFD model description: geometry, mesh, main hypotheses as well as the simulations methodology), secondly, the obtained numerical results are shown and discussed and finally, the main conclusions are presented.

2. Material and method

CFD modelling based on Unsteady Reynolds-Averaged Navier-Stokes equations (URANS) is used to model the airflow and CO_2 dispersion in a set of scenarios representing different configurations of terraces ranging from fully outdoor terraces to fully closed terraces including several semi-indoor cases.

The advantages of using this technique are:

● it is accurate enough to analyze the average behavior during the steady-state
● it involves reasonable computation times to compare a large number of scenarios.

2.1. Setup and description of simulated scenarios

A 3D geometric model of a real terrace has been done. The terrace is a parallelepiped which surfaces, S, is 32 m^2 and its height, H, is 2.85 m. It is considered representative of a typical terrace [44]. It is located in the center of a cylindrical domain with dimensions 15H radius and a domain height of 10H (Fig. 1).

The domain dimensions have been set according to the best practice guideline of [45]. The terrace tables and chairs have been taken from a free 3D model [46] and they have been arranged following an inline configuration. People inside the terrace are sitting and talking, as shown in Fig. 1. 3D people models have been obtained from Ref. [47]. The total number of persons is equal to 8 persons,
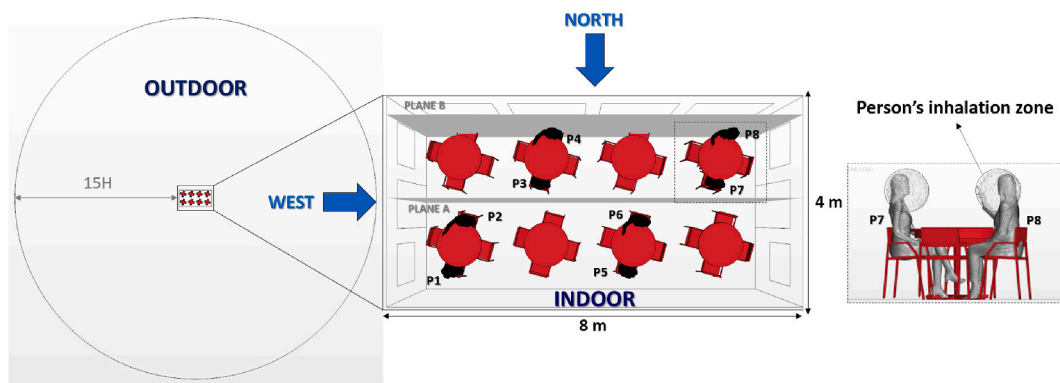

Fig. 1. Geometric model: left) domain dimensions; center) zoom in the terrace and layout of the people inside the terrace. Note that blue arrows represent the studied inlet wind directions; right) zoom of two partners (dotted circles represent the inhalation (intake) zones around the people).

denoted as Pi with $i = 1, 2, ..., 8$, and interpersonal distance between non-partners (people sitting around different tables) is greater than 2 m. The inhalation zone of each person has been delimited by a sphere of 50 l centered in her mouth, as shown in Fig. 1).

Up to $3H$ height, the mesh model is made by polyhedral cells of typical volume size, ΔV, equal to 1 m³. On surfaces, typical sizes, ΔS, range from 0.5 m² around the terrace enclosures, tables and chairs up to 0.1 m² around the people (see Fig. 2), but certain refinements have been added where surfaces have demanded it, which minimum surface size range from 0.1 m² around the terrace enclosures, tables and chairs up to 0.02 m² around the people. Finally, a 0.1 m thick prism layer has been applied on the ground (both outdoor and indoor) and on both faces of the terrace enclosures (see Fig. 2). From $3H$ to $10H$, the meshing has been extruded using 15 layers, increasing the thickness with height to save on the total number of cells. The total number of cells is approximately $1.3 \ 10^6$.

This mesh model has been chosen according to the mesh test carried out (see § 2.2).

Regarding the physical model, the URANS turbulent approach (based on the concept of Reynolds averaging) has been applied with a time-step, Δt, of 0.1 s and 3 inner iterations per time-step. Closing the URANS equations is solved with the $\kappa - \varepsilon$ Two-Layer model and the flexibility of the All Y+ wall hybrid treatment. The $\kappa - \varepsilon$ models provide a good compromise between robustness, computational cost, and accuracy. In addition, they are commonly used to study the gaseous atmospheric pollutant dispersion in urban environments. For the free parameters of the turbulent model, here it has been used the default values of STAR-CCM+15.04.010® [48]. It is verified that with this Δt all simulations verify CFL number is lower than 1 in most of the domain. Air has been assumed to behave as an ideal gas.

People can be considered both infecting and susceptible people therefore, we simulate the exhaled CO_2.

The exhaled CO_2 by each person has been simulated as a tracer gas, i.e., as a passive scalar magnitude. Thus, for each person, Pi, the following transport equations are solved:

$$\partial_t C_{CO_2}(\overrightarrow{r}, t) + \partial_j \left(\rho \ u_j \ C_{CO_2}(\overrightarrow{r}, t) - \frac{\mu_t}{Sc_t} \ \partial_j C_{CO_2}(\overrightarrow{r}, t) \right) = S_{C_{CO_2}} \quad j = x, y, z \tag{1}$$

where $C_{CO_2}(\overrightarrow{r}, t)$ is the CO_2 concentration in $\overrightarrow{r}$ and t from Pi, ρ is the air density, u_j the j-component of velocity, μ_t is the turbulent viscosity, Sc_t is the turbulent Schmidt number and $S_{C_{CO_2}}$ is the CO_2 exhaled by Pi. The advantage of using Pi equations is because it allows quantifying the influence of each infecting people.

Here, we have assumed that 5% by volume of exhaled air for each Pi is CO_2. It is exhaled through the mouths at a 37 °C and at approximately 0.37 m s⁻¹ (the mouths' surface is approximately 0.000 4 m²). The velocity direction is perpendicular to the mouths' surface so, it depends on the people's surface meshing. The assumed velocity is coherent with literature [49] and is equivalent to assume that an adult person exhales 0.5 l of air in each exhalation and has an emission rate at talking of 18 exhalations per minute. Note that, no other CO_2 sources have been considered.

Finally, Sc_t have been assumed equal to 0.7 [50–52].

The boundary conditions have been:

● outdoors, a logarithmic profile for the wind speed (u) and the typical forms for turbulent kinetic energy (κ) and dissipation rate (ε) for neutral profiles [53].

$$u(z) = \frac{u_*}{\kappa} \cdot \ln\left\{ \frac{(z + z_0)}{z_0} \right\}, \quad \kappa = \frac{u_*^2}{\sqrt{C_\mu}}, \quad \varepsilon = \frac{u_*^3}{(\kappa \cdot (z + z_0))} \tag{2}$$

where u_* is the friction velocity, z_0 is the roughness length, C_μ is a model constant ($= 0.09$) and κ is von Karman's constant ($\kappa = 0.4$). The considered meteorological conditions have been: 1.6 m s⁻¹ at 10 m-height (a relatively weak wind) and 7 °C, usual winter weather conditions in Madrid [54]. The ground is considered an adiabatic roughness surface with $z_0 = 0.03$ m.

● indoors, adiabatic smooth surfaces except for the people, who have been assumed to be at 23 °C. This internal heat gain is equivalent to assuming an average CLO (Clothing insulation) of 0.7 [55], an average MET (Metabolic rate) of 1.5 [56] an average surface area of 1.55 m² [57] and 75% thermal losses [58]. The radiative effects of people have been neglected versus the convective effects.
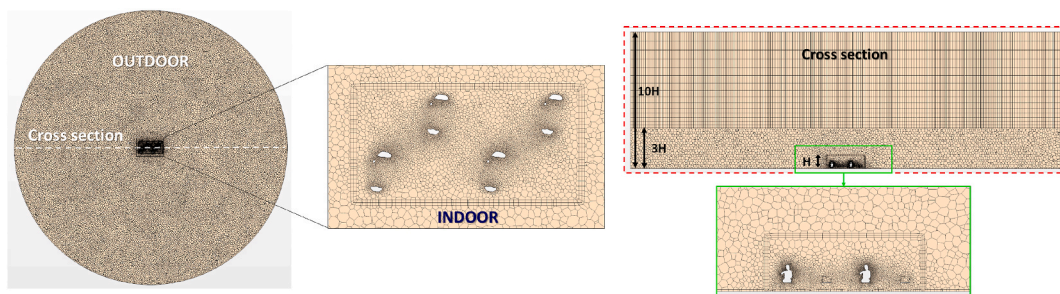

Fig. 2. Mesh model: left) horizontal view of the geometric domain at 1 m-height, both indoor and outdoor, and zoom inside the terrace and right) cross-section of the entire geometric domain and meshing detail inside the terrace.

This modelling approach has been previously applied to real urban environments and validated using experimental data of: NO$_2$, measured in a network AQMS (Air Quality Monitoring Stations) and using microsensors [59], and BC (Black Carbon), using an aethalometer respectively [60].

The simulated scenarios are shown in Fig. 3. The scenarios are defined considering different surfaces of the terrace open. They range from all surfaces open (Scenario 0) to all surfaces closed (Scenario 4), which represent typical terrace configurations in Spain. It is noteworthy that the airflow can enter and exit through the open surfaces since it is simulated not only the terrace but also the nearby environment, i.e. there is not any boundary condition imposed at the open surfaces.

Before people's CO$_2$ emissions are run, the free stream is initialized up to wind flow reaches the steady-state at time t_0. Then, CO$_2$ concentration is constant and equals to the background. At t_0, people's CO$_2$ emissions are run up to concentrations achieve the steady-
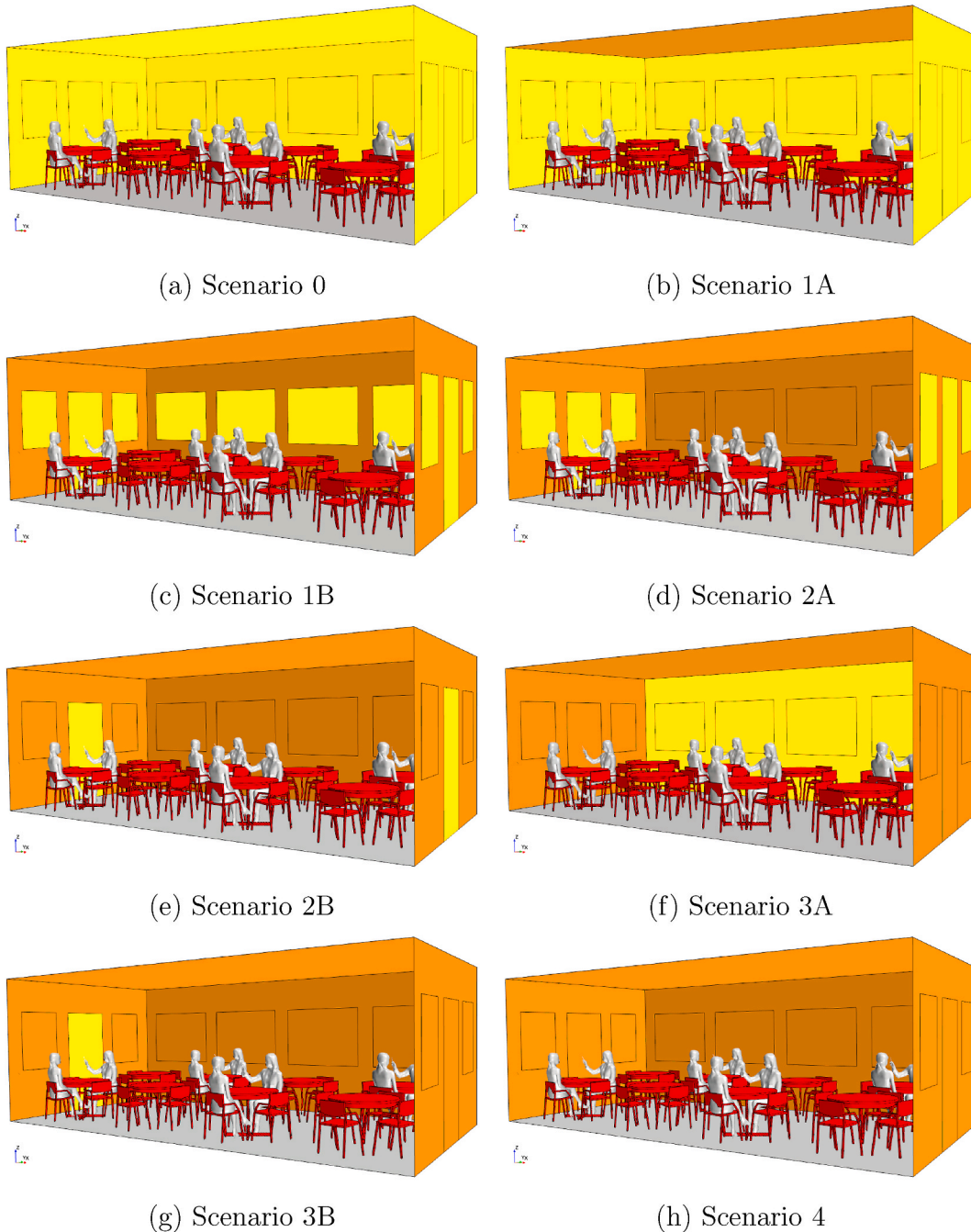

Fig. 3. Set of virtual scenarios (open surfaces in yellow and closed surfaces in orange). Note that it has been assumed that the terrace is attached to a building, except in Scenario 0. Therefore, there is always a front-side surface which is not shown in the pictures to see inside the terrace.

(a) Scenario 0 (b) Scenario 1A (c) Scenario 1B (d) Scenario 2A (e) Scenario 2B (f) Scenario 3A (g) Scenario 3B (h) Scenario 4

state, which is the main focus of this study (except in Scenario 4, an intrinsically unsteady and fully indoor terrace). From t_0, the distribution of CO_2 concentration in the terrace is heterogeneous and different from the background (ΔC_{CO_2}) depending on the scenario. Two wind directions have been considered: West (W) and North (W) (see Fig. 1), representing two extreme cases of incident wind flow regarding the terrace configuration: the first one longitudinally and the second one transversely. The model convergence during the steady-state is guaranteed because all conservation equations residuals are constant and less than 10^{-6}.

2.2. Mesh test

Scenario 2B has been chosen to carry out the mesh test. Three meshes are considered (*Mesh_fine*, *Mesh_medium*, and *Mesh_coarse*) which typical sizes are summarized in Table 1, has been applied.

For West wind direction, indoor profiles, calculated as surface averages every 0.1 m-height, of ΔC_{CO_2}, temperature (T), velocity (u), and turbulent kinetic energy (κ) have been compared (Fig. 4).

As can be seen, from a qualitative point of view, the three meshes adequately reproduce the trends but, from a quantitative point of view, there are differences between them. To evaluate these differences, the statistical parameters: correlation coefficient, R, normalized mean square difference, *NMSD*, root mean squared difference, *RMSD*, and fractional bias, *FB*, have been used considering the *Mesh_fine* results as a reference because they are the most accurate. Results are shown in Table 2.

As expected, there is a good agreement in both cases, with high values of R. But, *NMSD* and *RMSD* values are slightly higher in *Mesh_coarse* than in *Mesh_medium*, except for T, where the differences between meshes are negligible. Note that, the negative *FB* values indicate a general overestimation, which occurs in both cases, but more clearly in *Mesh_coarse* (except for T).

The few differences between *Mesh_medium* and *Mesh_fine* indicate that *Mesh_medium* resolution is good enough since increasing its resolution does not significantly improve the results. Therefore, *Mesh_medium* meshing seems a good compromise and hence it is then used for this study.

3. Results and discussion

Wind direction effect on the exposure to SARS-CoV 2 has been analyzed from the global to the local point of view using:

- the indoor volume average of ΔC_{CO_2}
- the indoor surface average of ΔC_{CO_2} at 1.2 m-height (onset of breathing zone)
- the volume average of ΔC_{CO_2} incoming to each person, Pi, from the others.

The first and second ones are associated with collective exposure and the third with individual exposure.

Unsteady simulations are run until the steady-state is reached. Firstly, the analysis of the results associated with the collective exposures has been carried out considering both unsteady and steady-state periods of simulations. For all scenarios, the steady-state is reached relatively fast (less than 1 h and most of them in few seconds), and for this reason, secondly, the results associated with both collective and individual exposures have been analyzed during the steady-state.

3.1. Wind direction effect on the collective exposure to SARS-CoV 2 in outdoor and semi-indoor scenarios

In Fig. 5, the time evolution of indoor volume average of ΔC_{CO_2} in each scenario is shown for both inlet wind directions (West and North) and, in Fig. 6, the time evolution of surface average of ΔC_{CO_2} at 1.2 m high for each scenario is also shown for both inlet wind directions. Each scenario has been classified according to its Air Changes per Hour (*ACH*) during the steady-state. This parameter is commonly used to study the indoor air quality [61] and here has been calculated from numerical results as:

$$ACH = \frac{3600}{\rho \cdot V} \sum_i^n \oint_{S_i} \dot{m}_{i,out} dS_i \tag{3}$$

where $\dot{m}_{i,out}$ is the outlet mass flow rate through each terrace open surface S_i, ρ is the air density (calculated at 25 °C and 1 atm) and V is the terrace volume.

It is observed that, as *ACH* decreases,

- the unsteady-state period increases from few seconds in the best-ventilated scenarios ($ACH \geq 444$) to less than 1 h in the worst-ventilated scenarios ($ACH \leq 6$).
- in general, and with exceptions, indoor volume average of ΔC_{CO_2} and surface average of ΔC_{CO_2} at 1.2 m increase at the steady-state.

Table 1
Summary of meshing characteristics.

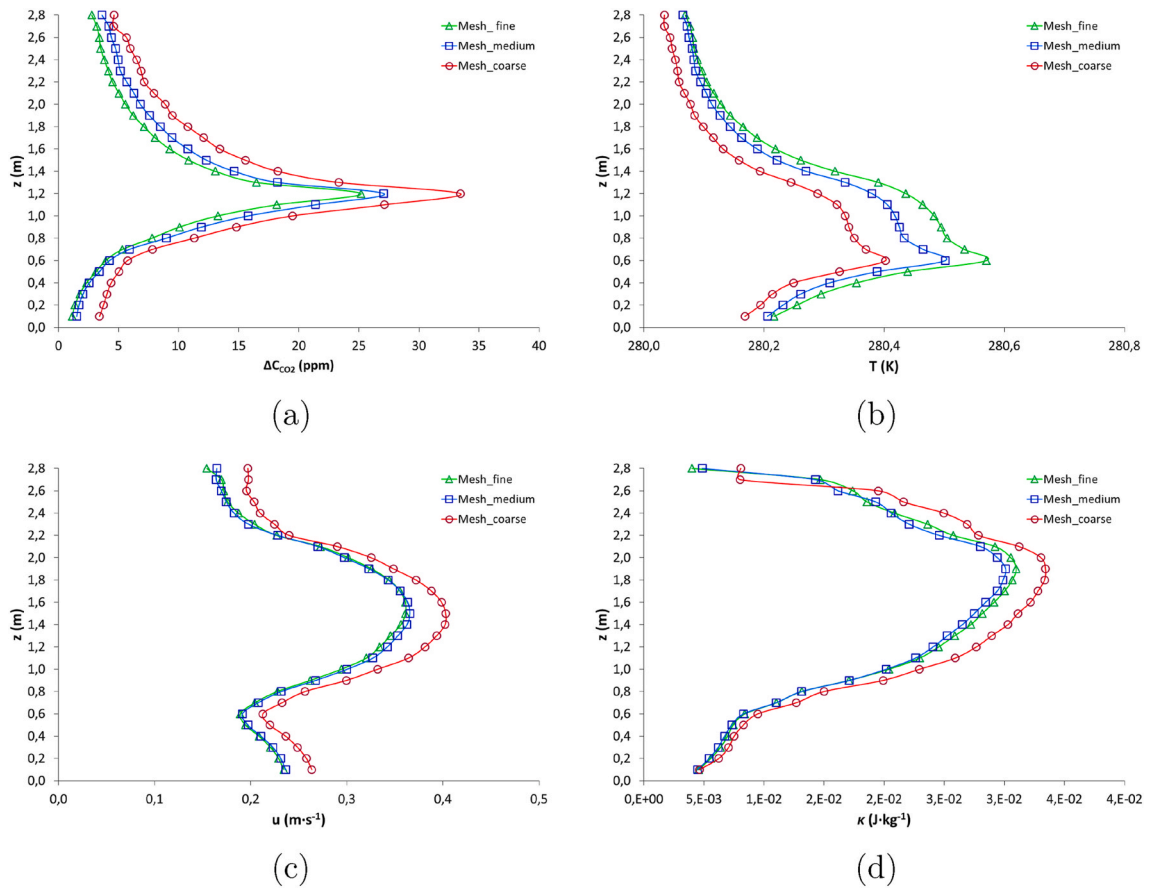| Mesh		Coarse	Medium	Fine
Total number of cells		310 301	1286 223	6399 519
ΔV (m^3)		2	1	0.5
ΔS (m^2)	Terrace enclosures and tables/chairs	1	0.5	0.25
	People	0.2	0.1	0.05
Refinement (m^2)	Terrace enclosures and tables/chairs	0.2	0.1	0.05
	People	0.04	0.02	0.01
Prism layer thickness (m)		0.2	0.1	0.05

Fig. 4. Indoor vertical profiles for Scenario 2B and West wind direction for: a) ΔC_{CO_2}, b) T, c) u and d) κ.

Table 2
Statistical parameters comparing Mesh_fine results with Mesh_medium and Mesh_coarse results for ΔC_{CO_2}, T, u and κ.

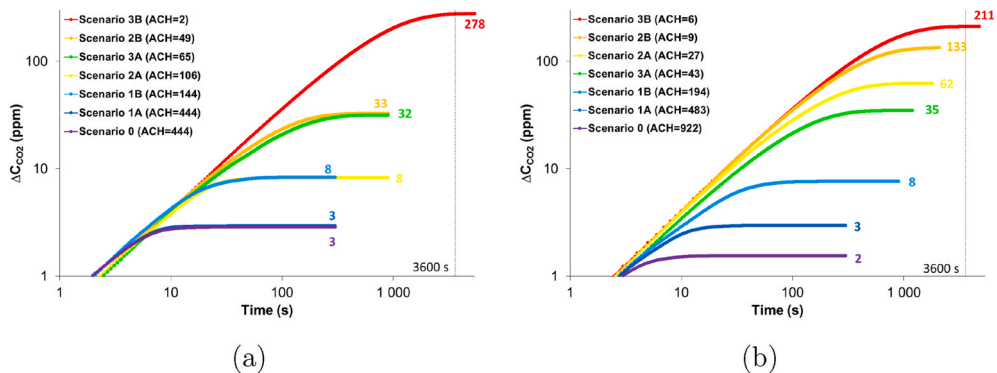|	Mesh medium				Mesh coarse			
	R	NMSD	RMSD	FB	R	NMSD	RMSD	FB
ΔC_{CO_2}	0.998	0.031	1.371	−0.154	0.997	0.216	4.082	−0.403
T	0.999	0.000	0.041	0.000	0.995	0.000	0.101	0.000
u	0.998	0.000	0.005	−0.007	0.994	0.014	0.032	−0.113
κ	0.999	0.001	0.001	0.023	0.984	0.019	0.003	−0.099

Fig. 5. Time evolution of indoor volume average of ΔC_{CO_2} for different Scenarios for a) West wind direction and b) North wind direction.
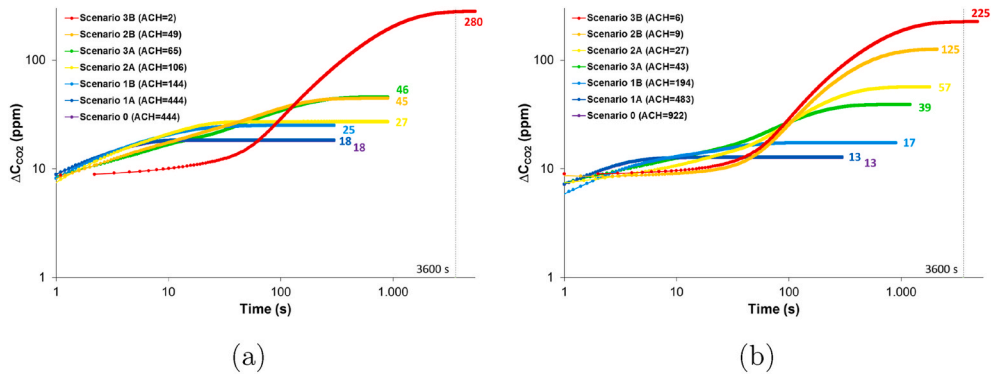
Fig. 6. Time evolution of surface average of ΔC_{CO_2} at 1.2 m high for different Scenarios for a) West wind direction and b) North wind direction.

But, these general considerations need to be particularized.

3.2. Wind direction effect on the individual exposure to SARS-CoV 2 in outdoor and semi-indoor scenarios

Analyzing the steady-state phase, depending on whether wind direction has an impact on indoor volume average of CO_2 or not, two cases are distinguished:

3.2.1. Cases where wind direction has no impact on indoor volume average of ΔC_{CO_2}. Scenarios 0, 1A and 1B, ACH $\geq$ 144

In Scenarios 0 and 1A (a completely outdoor terrace without any enclosure and a covered outdoor terrace with a top, respectively), the volume average of ΔC_{CO_2} is low (threshold value of [2–3] ppm), which means that outdoor, bioaerosols are well diluted in the air. But, this phenomenon is not isotropic and it depends on the source distance. In fact, ΔC_{CO_2} locally can take values equal to 0 ppm (no risk) or greater to 0 ppm (certain risk), especially around people's mouths, as it is shown in Fig. 7a) and b), c) and d). Considering the volume average of ΔC_{CO_2} incoming to each person from the others as the individual relative exposures of the people, it is observed that these exposures are greater when the susceptible is located inside the slipstreams from other people and when the susceptible is closer to the emitter. These results are in line with those obtained [62].

For Scenario 1B (a semi-indoor terrace with two facing doors and both, side and front-side, windows open), the volume average of ΔC_{CO_2} is the same for both wind directions, nonetheless the surface averaged of ΔC_{CO_2} at 1.2 m-height is different depending on wind direction due to the differences between the indoor vertical distributions of ΔC_{CO_2}. In Fig. 8 comparison between indoor profiles of ΔC_{CO_2} for both wind directions are shown.

The in-line people arrangement and rectangular terrace shape give rise to a cleaner people's breathing zone for North wind direction than for West wind direction and thus the indoor surface average of ΔC_{CO_2} at 1.2 m-height is 1.5 times lower for the North than for the West. Besides, due to building wall effects where the terrace is attached, while for North wind direction the exhaled CO_2 tends to accumulate more in the lower part of the terrace than in the upper part, for West wind direction the opposite happens.

These local flow patterns have a significant impact on the individual relative risk of SARS-CoV 2 transmission.

As can be seen in Fig. 7e) and f), depending on the wind direction, people with higher individual relative exposure to the exhaled CO_2 by other people are different: while for West wind direction the most exposed people are P8, P7, P5, and P6, for North wind direction they are P1, P3, P5, and P7 (see Fig. 1 for people numbering).

Finally, to have an overview of the local conditions, the volume average of ΔC_{CO_2} incoming to Pi from the others for both wind directions based on the people arrangement inside the terrace, i.e., as a function of the distance, is shown in Fig. 9.

The local flow patterns influence on the individual relative exposure in Scenario 1B is appreciated through two peaks, observed at 1 m (in close proximity) and 4 m (in proximity) respectively (Fig. 9). The first one, associated with Scenario 1B–N, shows a greater fluctuation in susceptible exposure than the second one (associated to Scenario 1B–W), indicating the variety of local conditions that can occur in close proximity depending on the people arrangement and orientation: facing or back to airflow.

3.2.2. Cases where wind direction has impact on indoor volume average of ΔC_{CO_2}. Scenarios 2A, 2B, 3A and 3B, ACH < 144

1. Scenarios where wind direction has a **high impact** on ventilation: Scenarios 2A and 2B.

In Scenario 2A (a semi-indoor terrace with side doors and side windows open but front-side windows closed) and Scenario 2B (a semi-indoor terrace with only both side doors open), while for West wind direction indoor volume average of ΔC_{CO_2} is 8 ppm and 33 ppm respectively for North wind direction is 35 ppm and 133 ppm respectively (i.e., the indoor volume average of $\Delta C_{CO_{2,N}} \approx 4$ times indoor volume average of $\Delta C_{CO_{2,W}}$). In these scenarios, it is verified that: $ACH_N < ACH_W$.

This is due to when airflow is perpendicular to terrace openings: doors and side windows in Fig. 10 a) and doors Fig. 10 c), the wind blowing from the West, the outdoor pressure gradient (positive pressure on the windward side and negative pressure on the leeward side) generates a wind-driven flow which favors indoor air is continuously withdrawn and replaced by fresh air, i.e., it favors the exhaled CO_2 horizontal transport from indoor to outdoor. This configuration is commonly known as efficient cross ventilation and here is characterized by a well-defined air current from the left side to the right side and relatively high indoor velocities (up to 2.03 m s^{-1} in

(a) Scenario 0-W

(b) Scenario 0-N

(c) Scenario 1A-W

(d) Scenario 1A-N

(e) Scenario 1B-W

(f) Scenario 1B-N

(g) Scenario 2A-W

(h) Scenario 2A-N

(i) Scenario 2B-W

(j) Scenario 2B-N

(k) Scenario 3A-W

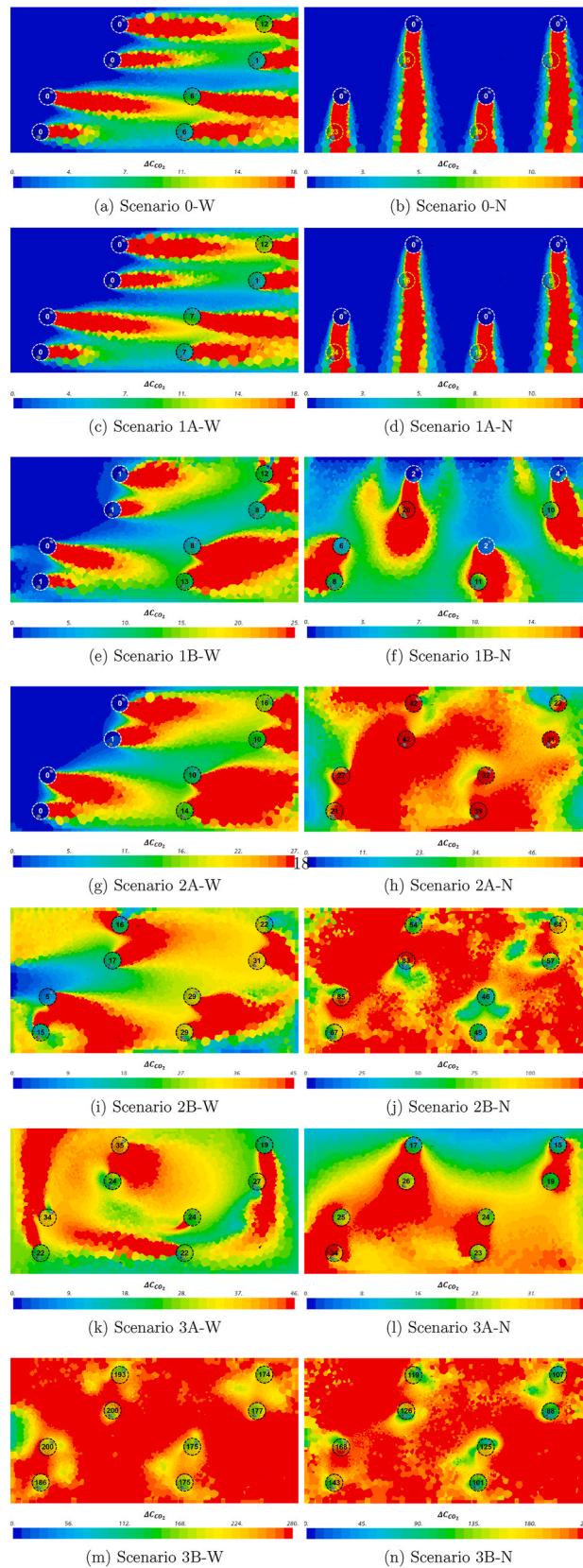(l) Scenario 3A-N

(m) Scenario 3B-W

(n) Scenario 3B-N

Fig. 7. ΔC_{CO_2} distribution at 1.2 m-height (onset of breathing zone) and volume average of ΔC_{CO_2} incoming to each person from the others (dotted circles) in different scenarios for West (W) and North (N) wind directions. Note that red color indicates values higher or equal than the top values of their respective scales, which correspond to the indoor surface average ΔC_{CO_2} at 1.2 m-height of each case during the steady-state. The open areas (doors and windows) of each scenario can be observed in Fig. 3.
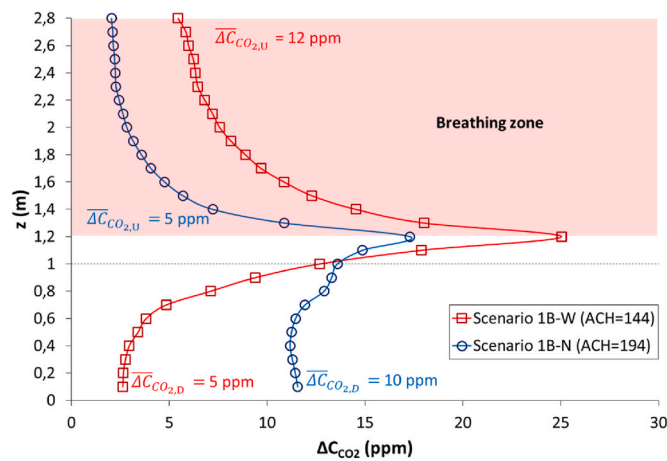

Fig. 8. Indoor vertical profiles of ΔC_{CO_2} in Scenario 1B for both wind directions. $\overline{\Delta C}_{CO_2, U or D}$ represent the average values of indoor surface averages of ΔC_{CO_2} up to 1 m-height and from 1 m-height to the top respectively.
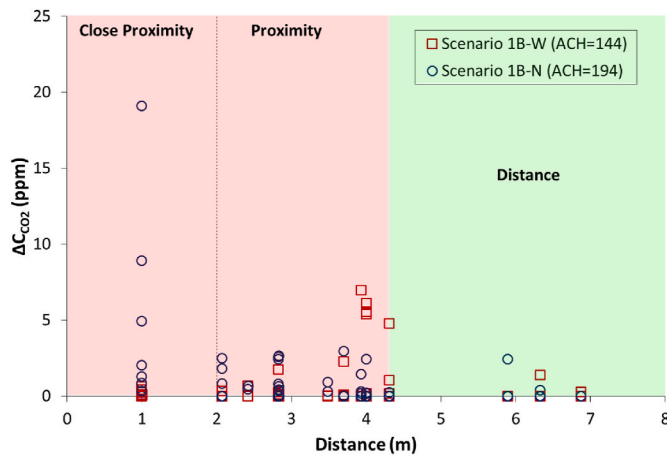

Fig. 9. Volume average of ΔC_{CO_2} incoming to Pi from the others in Scenario 1B for both wind directions as a function of the distance.

both scenarios, see Fig. 10 a) and c). Whereas, when airflow is parallel to terrace openings: doors and side windows in Fig. 10 b) and doors in Fig. 10 d), wind blowing from the North, only local pressure gradients occur which cause a weak airflow through the openings. This stagnation effect favors the exhaled CO_2 remains inside the terrace. This configuration is characterized by air currents flowing in and out at the same time and relatively low indoor velocities (as maximum 0.30 m s^{-1} in Scenario 2A, Figs. 10 b), and 0.29 m s^{-1} in Scenario 2B, Fig. 10 d)).

The effects of cross ventilation are also observed in Fig. 11, where the comparison between indoor profiles of ΔC_{CO_2} in Scenarios 2A and 2B for both wind directions are shown. It is observed how the cross-ventilation can completely inhibit CO_2 stratification inside the terrace when $ACH = 106$ (Scenario 2A-W) and it can prevent that exhaled CO_2 concentrations in the upper part of the terrace exceed exhaled CO_2 concentrations at 1.2 m-height when $ACH = 49$ (Scenario 2B–W). The lack of effective ventilation as ACH value decreases gives rise to the CO_2 concentrations in the upper part of the terrace exceed CO_2 concentrations at 1.2 m-height and the typical shape of indoor profiles of CO_2 goes from being quasi-linear to sigmoidal, which happens for the North wind (parallel to the open surfaces).

Note that, similar shapes of indoor profiles are obtained for T, as shown in Fig. 12. Thus, it is easy to deduce that, in conventional semi-indoor terraces, is necessary a compromise between ventilation performance and thermal comfort.

For Scenario 2B, the average relative exposure to SARS-CoV 2 for West wind direction is lower than for North wind direction: 21 ppm versus 62 ppm, due to the ventilation difference. But flow patterns provide very different individual relative exposure between
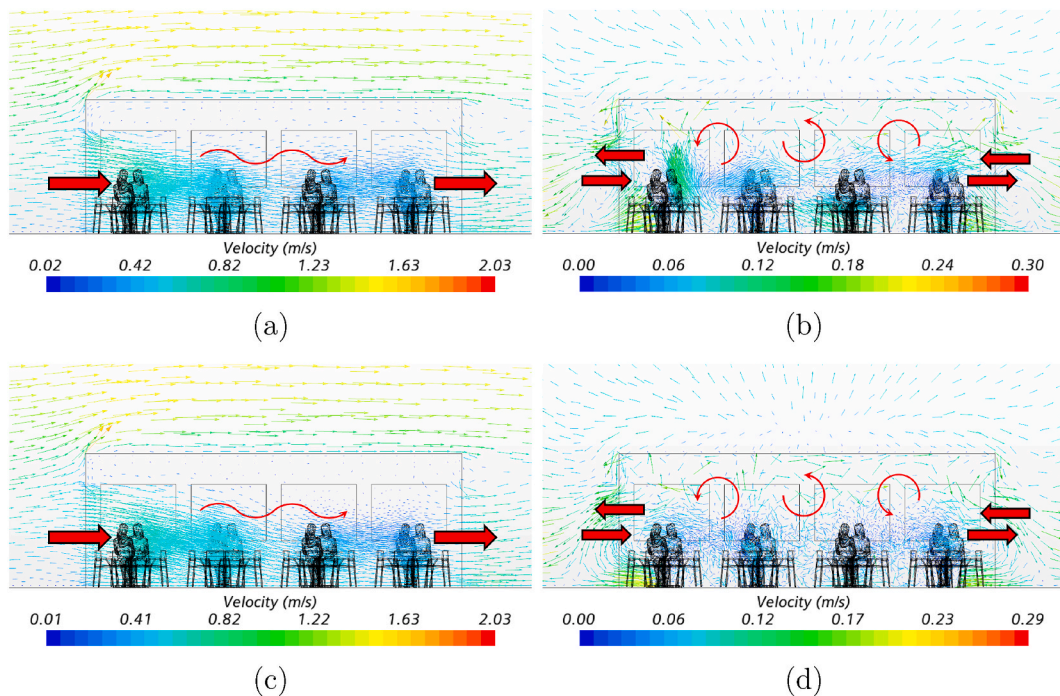
Fig. 10. The tangential component of the velocity field on plane A (a section in the middle of the terrace perpendicular to both doors along West wind direction, see Fig. 1) for a) Scenario 2A-W, b) Scenario 2A-N, c) Scenario 2B–W and d) Scenario 2B–N. The overlapping red arrows represent the airflows through the inlets/outlets and inside the terrace.
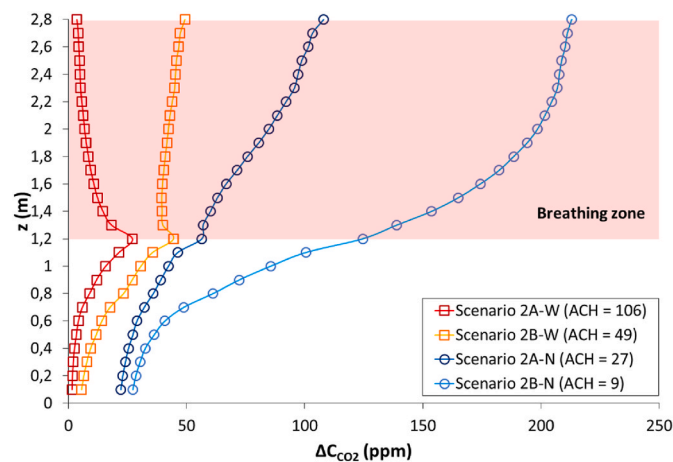

Fig. 11. Indoor vertical profiles of ΔC_{CO_2} in Scenarios 2A and 2B for both wind directions.

people, as can be appreciated in Fig. 7i) and j). For West wind direction (a cross ventilation scenario), ΔC_{CO_2} high-resolution map at 1.2 m-height shows strong heterogeneity (higher CO_2 concentrations downstream than upstream of people), which yields a maximum percentage difference in individual relative exposure between people upstream and downstream of 84%. However, for the North wind direction, there is not a well-defined flow removing CO_2 and therefore the exhaled CO_2 remains mixed inside the terrace, which makes the ΔC_{CO_2} high-resolution map more homogeneous and with higher concentrations as the exhaled CO_2 is accumulated. In this case, the maximum percentage difference in individual relative exposure between people is 47%.

Furthermore, if individual relative exposure to SARS-CoV 2 is analyzed based on the people arrangement inside the terrace, it is possible to better understand the flow patterns' impact. In Fig. 13, volume average of ΔC_{CO_2} incoming to P8 from the others as a function of the distance between them is shown as an example. In both cases, from 4 m, the risk decreases with the distance. But, at distances less than 4 m (in proximity), there are strong differences. While in Scenario 2B–N, the exposure is mainly due to the presence of P7, P6, and P5 (especially P7 which is located less than 2 m from P8, in closed proximity), in Scenario 2B–W (cross ventilation), in
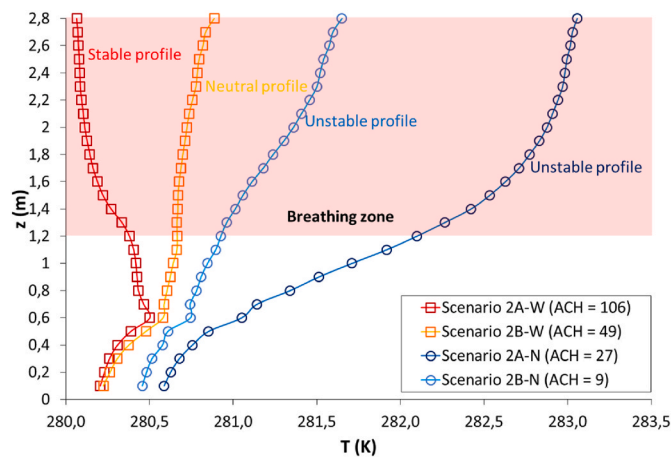
Fig. 12. Indoor vertical profiles of T in Scenarios 2A and 2B for both wind directions.

proximity there is hardly any exposure, but at distance, the exposure is slightly higher than that of Scenario 2B–N. This is due to the airflow connecting P8 with P3 and P4. Depending on the Reproductive Number (R_0) of the new SARS-CoV 2 variants and the cross ventilation flow rate, this situation could be classified as of potential risk, as it is also stated by Ref. [63] in their research on a naturally ventilated hospital ward.

Lastly, to provide a global view regarding the individual relative exposures for Scenario 2B, in Fig. 13, the volume average of ΔC_{CO_2} incoming to the rest of the people Pi are also shown as a function of the distance.

Although wide fluctuations in ΔC_{CO_2} are also observed for Scenario 2B–N, unlike Scenario 1B–N, the exposure between 1 m and 4 m is quite similar. For this reason, in shared and poorly ventilated settings it is recommended to increase the ventilation to prevent the short-range airborne transmission, which is much higher than the long-range airborne transmission.

2. Scenarios where wind direction has a **medium impact** on ventilation: Scenario 3A.

In Scenario 3A (a semi-indoor terrace without front-side enclosures), while for West wind direction indoor volume average of ΔC_{CO_2} is 32 ppm for North wind direction is 62 ppm (i.e., the indoor volume average of $\Delta C_{CO_{2,N}} \approx 2$ times indoor volume average of $\Delta C_{CO_{2,W}}$). In this scenario, it is also verified that $ACH_N < ACH_W$.

When wind flow is parallel to the terrace open surface, a clockwise vortex in a horizontal plane is created (see Fig. 14 a). This airflow, although is characterized by moderate indoor velocities (as maximum 0.71 m s^{-1}), promotes the CO$_2$ removal from terrace. However, when wind flow is perpendicular to the terrace open surface, there is not a pressure gradient between indoor and outdoor. For this configuration, the weak air currents generated close to the terrace open surface (as maximum 0.44 m s^{-1}), see Fig. 14 b), cause a poor mass flow exchange between indoor and outdoor. Therefore, here, CO$_2$ removal from the terrace is lesser.

Analyzing indoor profiles of ΔC_{CO_2} in Scenario 3A for both wind directions (Fig. 15), the influence of flow patterns in local behaviors arise again. Although for the North wind direction the exhaled CO$_2$ tends to provide higher concentrations in the terrace lower and upper parts than for the West wind case, the concentration at breathing zone is smaller.
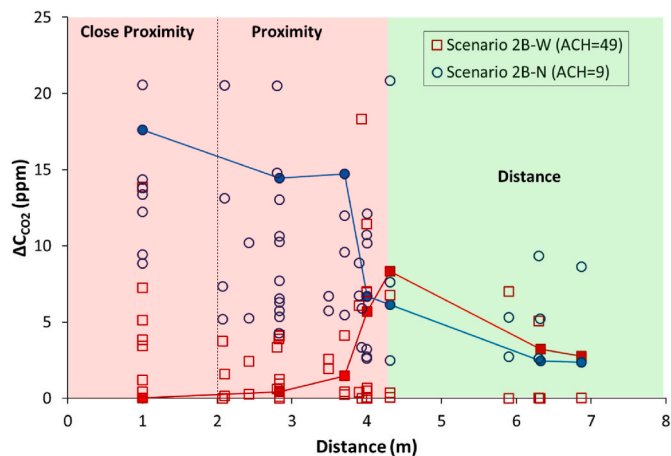

Fig. 13. Volume average of ΔC_{CO_2} incoming to P8 from the others (filled markers) and also to the rest of the people Pi (empty markers) in Scenario 2B for both wind directions as a function of the distance.
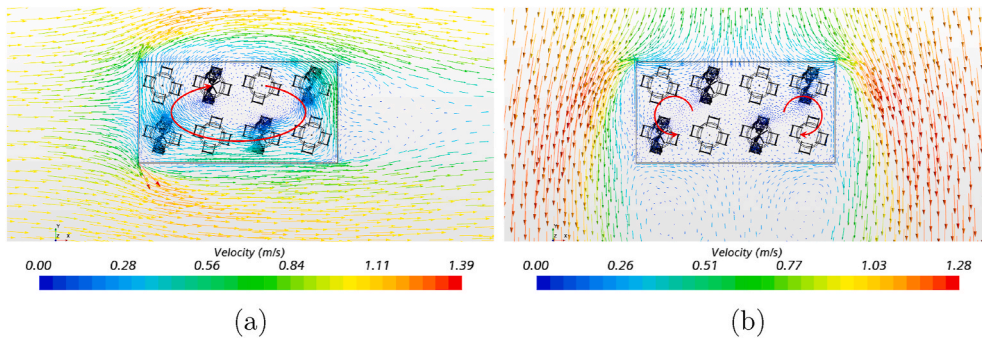
Fig. 14. The tangential component of the velocity field at 1.6 m-height in Scenario 3A for: a) West wind direction and b) North wind direction. The red arrows inside the terrace represent the air that flows inside the terrace and through the inlet/outlet.

Regarding the average relative exposure to SARS-CoV 2 is practically equivalent for both wind directions: 26 ppm (West) versus 22 ppm (North) and the maximum percentage difference in individual relative exposure between people also: 46% versus 56% respectively. Nevertheless the impact of flow patterns is observed in Fig. 7 k) and l).

3. Scenarios where wind direction has a **low impact** on ventilation: Scenario 3B.

In Scenario 3B (a semi-indoor terrace with only one side door open), while for West wind direction indoor volume average of ΔC_{CO_2} is 278 ppm for North wind direction is 211 ppm (i.e., the indoor volume average of $\Delta C_{CO_2,N} \approx$ indoor volume average of $\Delta C_{CO_2,W}$). In this scenario, it is also verified that: $ACH_N > ACH_W$.

In this scenario, for both wind directions, the indoor-outdoor exchange takes place through a unique surface: the left side door. This configuration is commonly known as single-sided ventilation and is characterized by a very limited exchange. For West wind direction, the airflow enters through the upper part of the door and leaves through its lower part, see Fig. 16 a), and for North wind direction, the air flows the opposite, see Fig. 16 b). But, between both cases, the first one has the most limited exchange.

This is due to when the airflow is perpendicular to the open door, wind blowing from the West, two vortexes are generated, see Fig. 16 a), one outside (clockwise) and another inside (counterclockwise) which block the exit of exhaled CO_2 from indoor to outdoor. Whereas when wind flow is parallel to the open door, wind blowing from the North, see Fig. 16 b), the local pressure gradient generated at the right side of the terrace between indoor and outdoor, allows a slight removal of exhaled CO_2. The maximum indoor velocities are, for West wind direction 0.22 m s^{-1} and for North wind direction 0.29 m s^{-1}.

The effects of the different indoor-outdoor exchanges can be also observed in Fig. 17, where surface average of ΔC_{CO_2} at any terrace height is higher for West wind direction than for North wind direction.

Although, in both cases, exhaled CO_2 concentrations in the upper part of the terrace exceed exhaled CO_2 concentrations at 1.2 m-height and the shape of indoor profiles of CO_2 is sigmoidal. That is why this configuration is not recommended and it is encouraged to increase the ventilation of these environments. Since, natural ventilation efficiency can be improved through features and/or elements such as the atrium, wind catcher, solar chimney, and window type [64,65], all of them could be possible solutions to explore.

Regarding the average relative exposure to SARS-CoV 2, for West wind direction is 198 ppm and for North wind direction is 122 ppm. These results are due to the ventilation difference.
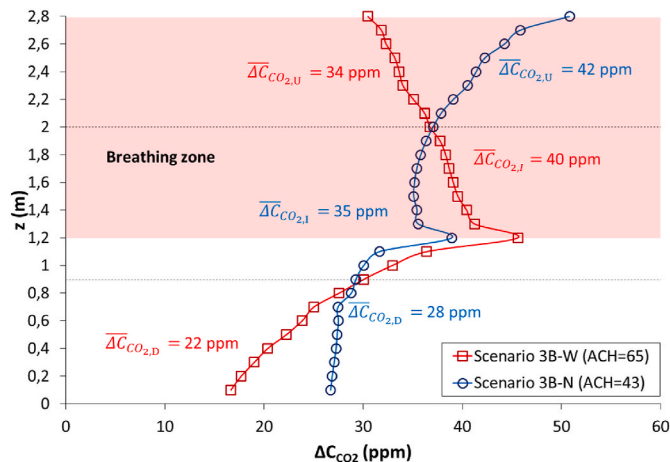

Fig. 15. Indoor vertical profiles of ΔC_{CO_2} in Scenario 3A for both wind directions. $\overline{\Delta C}_{CO_2,U,MorD}$ represent the average values of indoor surface averages of ΔC_{CO_2} up to 0.9 m, between 0.9 m and 2 m and between 2 m y 2.8 m-height respectively.
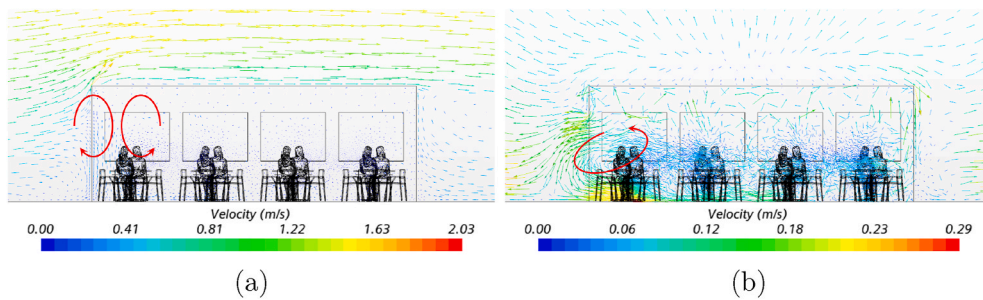
Fig. 16. The tangential component of the velocity field on plane A in Scenario 3B for a) West wind direction and b) North wind direction. The overlapping red arrows represent the air that flows inside the terrace and through the inlet/outlet.
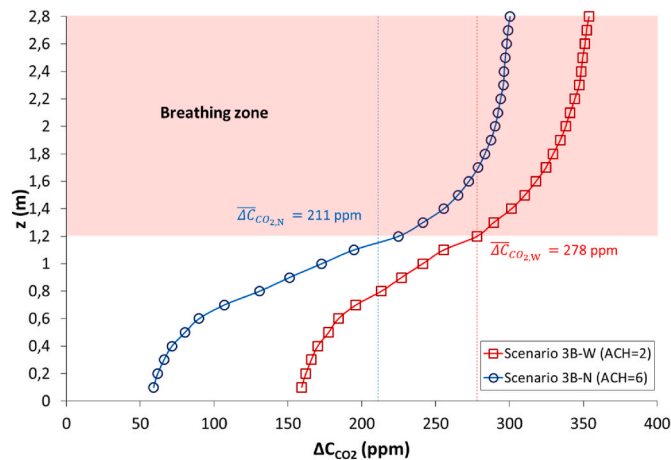

Fig. 17. Indoor profiles of ΔC_{CO_2} in Scenario 3B for both wind directions.

And regarding the maximum percentage difference in individual relative exposure between people, for West wind direction is 13% and for North wind direction is 48%. These results are due to the different mixing degrees, as shown in the ΔC_{CO_2} high-resolution map at 1.2 m-height of Fig. 7 m) and n), where homogeneity is greater for West wind direction than for North wind direction. Note that, for West wind direction, the average relative exposure to SARS-CoV 2 in Scenario 3B is 25 times higher than in Scenario 0 (outdoor environment) and for North wind direction is 15 times higher. These results are coherent with those obtained by Ref. [66].

The impact of flow patterns on the individual relative exposure to SARS-CoV 2 is important. In Fig. 18 streamlines from P2's mouth to the outlet are shown. The streamlines are employed to follow the path of the exhaled CO_2 by P2 into the bulk fluid. While, for West wind direction, the inlet flow forces the exhaled CO_2 by P2 goes through a huge part of the terrace before exits across the lower part of the door (i.e., it travels along pathway), for the North direction, the exhaled CO_2 by P2 immediately exits across the upper part of the door (i.e., it travels a short pathway). Therefore, it is reasonable to think that the influence of P2 on other people, especially on P1, depends on wind direction and will be higher in the first case than in the second. Note that the exhaled CO_2 rises because is hotter than the surrounding air, thus, it would be interesting to use this fact to redesign the terrace openings (low-tech modifications) in such a way
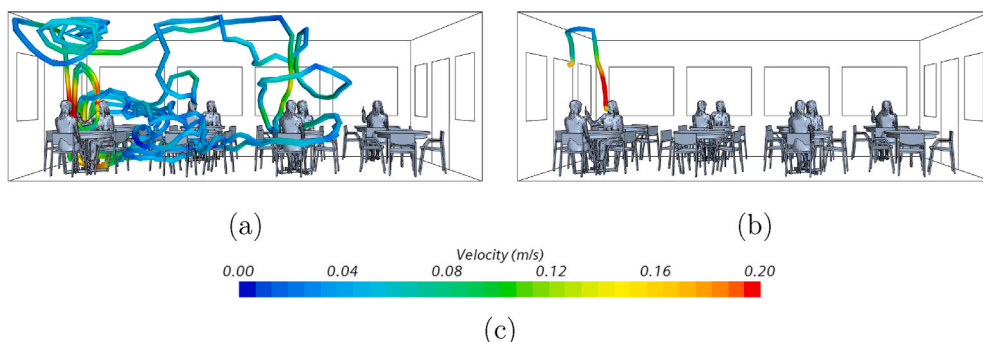

Fig. 18. Streamlines from P2's mouth to the outlet in Scenario 3B for both wind directions a) West wind direction and b) North wind direction.

the indoor CO_2 paths are as short as possible.

Finally, the overview of the volume average of ΔC_{CO_2} incoming to Pi from the others in Scenario 3B is shown in Fig. 19. Note that, on one hand, the mean exposure decreases with the distance between people, but the contribution from people at distance higher than 4 m is large (similar to people located in proximity) in some cases. On the other hand, the local flow patterns impact is appreciated through two maxima: at 1 m (in close proximity) and 4 m (in proximity) respectively, and similar maximum values for the rest of distances (both in proximity and distance). These results are analogous to those theoretical obtained by Ref. [33] and those experimental obtained by Ref. [67] in indoor environments (a classroom and an ICU respectively).

3.3. Comparison between semi-indoor scenarios with similar volume average of ΔC_{CO_2}

This section shows how equivalent scenarios from a spatial average concentration point of view, can be very different from a local concentrations point of view.

Comparison between Scenarios 2A-W and 1B–W and Scenarios 3A-W and 2B–W deserve special attention since, in both cases, volume averages of ΔC_{CO_2} are equal, 8 ppm and approximately 32 ppm respectively, but ACHs are different, see Fig. 5.

In addition, the contaminant removal effectiveness index, defined as the ratio between the average concentration of a contaminant at outlets and the average concentration of contaminant in the room during the steady-state, is computed for these scenarios. This index depends on the indoor flow patterns and the contaminant sources positions. If the airflow directly join the contaminant sources with the outlets it takes high values. But, if contaminant sources are in recirculating zones, it takes low values [68].

ΔC_{CO_2} at outlets is $\Delta C_{CO_2,out,2A} = 16$ ppm and $\Delta C_{CO_2,out,1B} = 11$ ppm for Scenarios 2A-W and 1B–W respectively. Therefore, the removal effectiveness index is greater for Scenario 2A-W than for Scenario 1B–W, indicating that, from the point of view of CO_2 removal efficiency of the complete terrace, Scenario 2A is more efficient than Scenario 1B. This is because, while in Scenario 2A-W, the exhaled CO_2 is rapidly removed by the generated flow pattern between side doors and windows (cross ventilation), Fig. 20 a), in Scenario 1B-W, exhaled CO_2, especially by people near the front side windows, remains indoors, accumulated in the upper part of the terrace, Fig. 20 b). In the last configuration, the streamlines curve from the left side towards the front side, generating a vortex in the upper left half of the terrace and a low-speed zone close to people located near to front side windows. The generated flow pattern weakens the cross ventilation and thus the exhaled CO_2 horizontal transport. The same was pointed by Ref. [69]; concluding that inlets/outlets location severely influences the ventilation efficiency.

Although this comparison shows the effectiveness of cross ventilation from the global point of view of the terrace, it is also analyzed from the local point of view. Fig. 7 g) and 7 e) show that, in both scenarios, the no exposed people (or donors) are P4, P3, P2, and P1 ($\Delta C_{CO_2} \leq 1$ ppm) and the exposed people (or receptors) are the P8, P7, P5 and P6 ($\Delta C_{CO_2} \geq 8$ ppm), because they are downstream of P4, P3, P2, and P1 respectively. But, the individual exposures of P8, P7, P5 and P6, are slightly higher for Scenario 2A-W than for Scenario 1B–W.

In the first scenario (cross ventilation), there is only a mainstream crossing the terrace (from the left side door and windows to the right side door and windows). However, in the second scenario there is a secondary stream, in addition to the mainstream, acting perpendicular to the mainstream (from the left side door and windows to the front side windows) and which inhibits the horizontal transport of CO_2 but favors the CO_2 vertical transport.

With this case, it is illustrated how in two equivalent scenarios from a global point of view, the removal effectiveness index is not decisive, or exclusively decisive, when evaluating individual exposure. Since, due to the flow patterns, in Scenario 2A-W mean people exposure is 14% greater than Scenario 1B–W, although it has a better removal effectiveness index.

Regarding the comparison between Scenarios 3A-W and 2B–W, in spite of the volume average of ΔC_{CO_2} is similar, the individual exposures are very different due to the different indoor flow patterns. For example, while P2 is the lowest exposed person in Scenario 2B–W, is one of the most exposed people in Scenario 3A-W, with an exposure increase of up to 85%. This is because, in Scenario 2B–W (cross ventilation), P2 is sited just in front of the inlet and therefore subjects to strong ventilation, but in Scenario 3A-W, the exhaled CO_2, mainly by P5, P7, and P8, it is efficiently transported from right side to left side by the airflow which pass thought all the terrace (Fig. 21). This case clearly illustrates how the transmission of respiratory diseases, like SARS-CoV 2, could be given at a distance. And, for this reason, in shared places with natural ventilation, it is advisable to use masks and to reduce the permanence time.

3.4. Effect of single-sided ventilation in a fully closed terrace on CO_2 concentration

To quantify the growth rate of CO_2 concentration when the terrace is completely closed and how rapidly the CO_2 concentration decreases when the terrace is reopened (or ventilated), the following numerical exercise has been carried out. Starting from the Scenario 3B during the steady-state:

1. The unique open surface (left side door) is closed, in such a way that Scenario 3B (semi-indoor) becomes Scenario 4 (indoor)
2. The model is run for 1-h recording the results of the dynamic simulation each time-step.
3. Then, the left side door is reopened, in such a way that Scenario 4 becomes Scenario 3B again
4. The model is run for 1 more hour recording the results of the dynamic simulation each time-step.

In Fig. 22, it is observed that indoor volume average of ΔC_{CO_2} growth rate for the completely closed terrace is linear (growing rate equivalent to 178 ppm/·hour) because infiltration is neglected. After reopening the left side door, the CO_2 concentration decays following the next function:

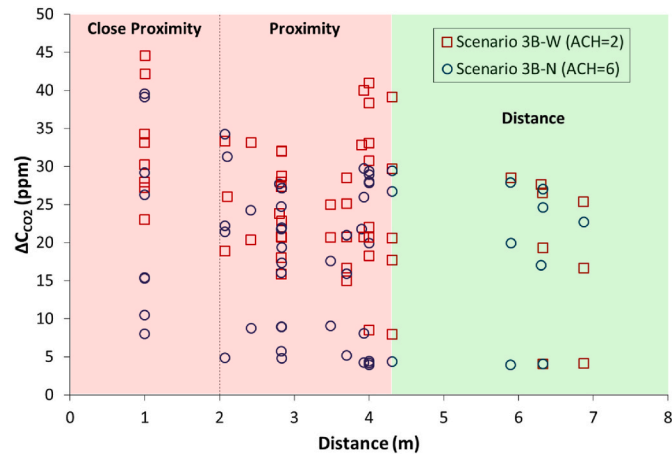$$\Delta C_{CO_2}(t) = C_1 + C_2\,e^{-\frac{t}{\tau}} \tag{4}$$

Fig. 19. Volume average of ΔC_{CO_2} incoming to Pi from the others in Scenario 3B for both wind directions as a function of the distance.
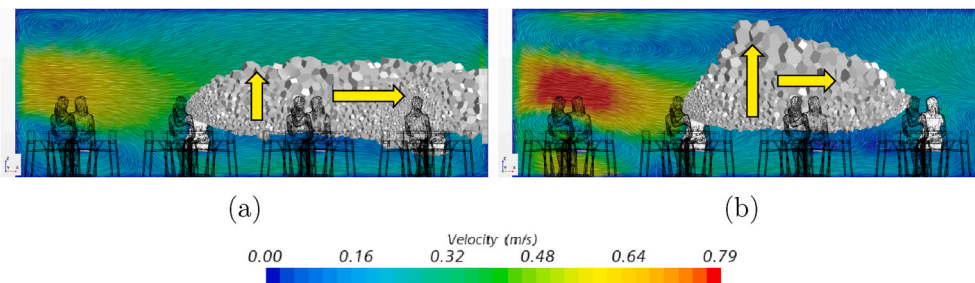

Fig. 20. Line integral convolution of the tangential component of the velocity field on plane B (a section along West wind direction close to North facade, see Fig. 1) and recreation of the exhaled ΔC_{CO_2} by P4 (cells in gray color, threshold used: $\Delta C_{CO_2} \leq 7$ ppm) for a) Scenario 2A-W and b) Scenario 1B–W. The overlapping yellow arrows represent the transport of the exhaled CO_2 by P4 inside terrace. The open areas (doors and windows) of each scenario can be observed in Fig. 3.

where C_1 and C_2 are the volume average of ΔC_{CO_2} concentrations in Scenario 3B during the steady-state and in Scenario 4 in 1 h respectively, the needed time to reach the steady-state, 5τ, is for West wind direction 3241 s and North wind direction 2767 s, due to the ventilation difference. This information can be relevant because the transmission of airborne infectious diseases may occur during the unsteady state [70].

Finally, the average relative exposure of SARS-CoV 2 in Scenario 4 in 1 h is: for West wind direction 1441 ppm and for North wind direction 1383 ppm, Fig. 23, which means that it is between 7 and 11 times higher than in respective Scenario 3A (with only one open door: that is the worst semi-indoor scenario). And, the maximum percentage difference in individual relative exposure between people is less than 5%, so, in this case, the assumption of a completely mixed flow inside the terrace would be appropriate.

4. Conclusions

Within the scope of the research, the following conclusions have been drawn:

1. In outdoor terraces, such as Scenarios 0 and 1A, little risk of transmission is envisaged except to short-range distances. But under certain meteorological conditions, the non-partners influence could be greater than the partners'.
2. In semi-indoor terraces, in general, the higher the ventilation (ACH value), the lower the average relative exposure to SARS-CoV 2. But also, it is advisable trying to minimize the impact of potential flow patterns created by the ventilation increasing. Particularly:
   (a) Wind-driven cross-ventilation (Scenarios 2A-W and 2B–W) can create healthy indoor environments from the global point of view, as [71] have already stated. But, depending on the induced airflow, some scenarios can contribute to effectively spread the exhaled bioaerosols by some people and causing infections at a certain distance away. That is why it is recommended to maintain the interpersonal distancing guidelines of 2 m even in well-ventilated environments like Scenarios 2A-W and 2B–W or 3A.
   (b) In poorly ventilated scenarios, the distance to what the relative exposure significantly decreases, increases, and in the worse cases there is no such distance because the exhaled CO_2 is well mixed throughout the room. For example, in Scenario 3B, short-range transmission is practically equal to long-range transmission. Therefore, the measures based on the social distance between people have a negligible impact on reducing the cross-infection risk in this type of environment. Instead, measures based on improvement and control of ventilation, the use of masks, and the reduction of exposure time become special importance.
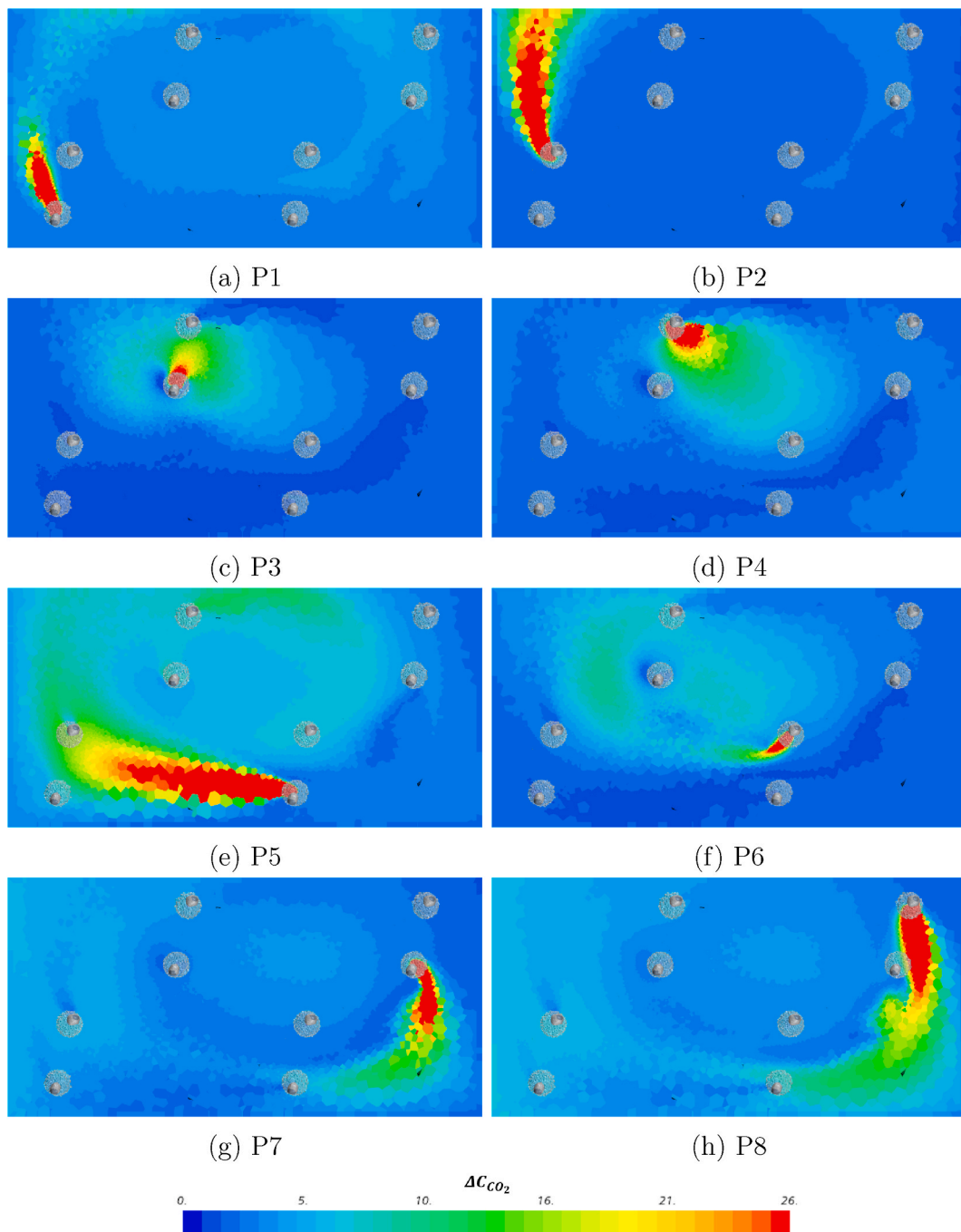
(a) P1   (b) P2

(c) P3   (d) P4

(e) P5   (f) P6

(g) P7   (h) P8

Fig. 21. ΔC_{CO_2} distributions at 1.2 m-height (onset of breathing zone) due to each Pi in Scenario 3A-W. Note that the red color indicates values greater or equal than the upper-value scale. The upper value corresponds with the average relative exposure to SARS-CoV 2.

3. Indoor terraces are critical because the air is completely mixed inside them. For example, in Scenario 4, the average relative exposure in 1 h is between 7 and 11 times higher than in the worst semi-indoor scenario.

4. Box models are only suitable for individual risk assessments in closed environments. For semi-indoor environments, airflows are complex and therefore distributions of CO_2 can be heterogeneous.

5. Comparison between different terraces (Scenarios 2A-W and 1B–W and Scenarios 3A-W and 2B–W) shows the importance of approaching the individual exposure to SARS-CoV 2 from the flow patterns between infectors and susceptibles point of view. The SARS-CoV 2 outbreaks reported by Refs. [31,72] (in a restaurant) and [73] (in a choral) have also evidenced this fact
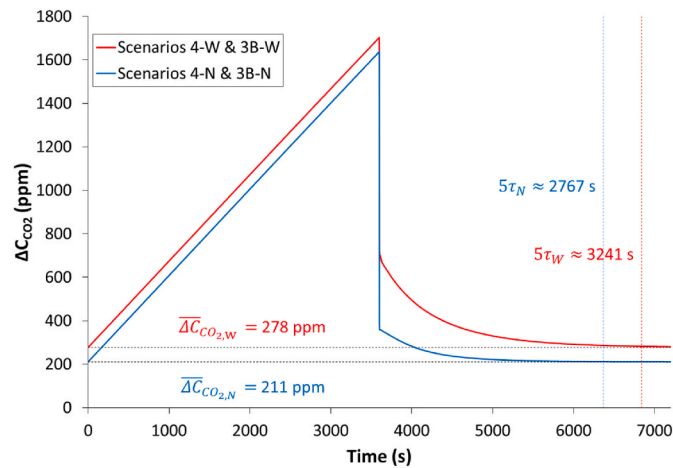
Fig. 22. Time evolution of indoor volume average of ΔC_{CO_2} for Scenarios 4-W and 4-N (from 0 s up to 3600 s) and for Scenarios 3B–W and 3B–N (from 3600 s to 7200s).
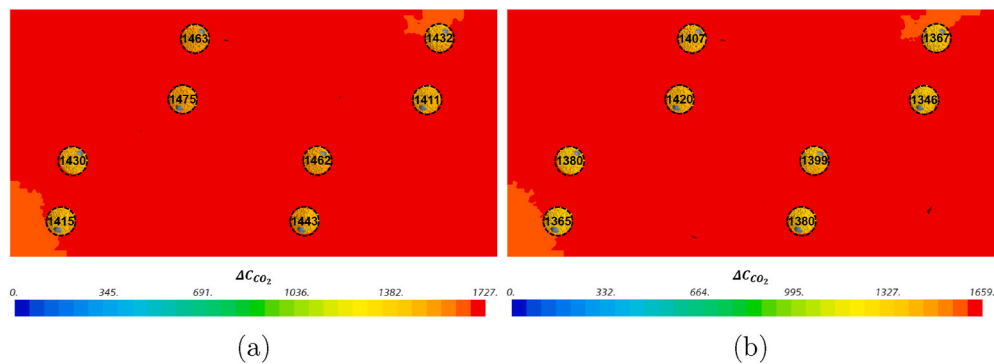

Fig. 23. ΔC_{CO_2} distributions at 1.2 m-height (onset of breathing zone) and volume average of ΔC_{CO_2} incoming to each person from the others (values dotted circles) in 1 h for a) Scenario 4-W and b) Scenario 4-N. Note that the red color indicates values greater or equal than upper values of respective scales. Upper values correspond with the indoor surface average of ΔC_{CO_2} at 1.2 m-height in 1 h.

6. Air quality indexes, such as CO_2 removal effectiveness, should be used with caution for estimating people exposure. In the analyzed case: two scenarios (2A-W and 1B–W) with the same volume average concentration, mean people exposure is higher for 2A-W than for 1B–W, which cannot be explained by means of this index since 2A-W has a better index than 1B–W. Future research work should be conducted about using air quality indexes for estimating people exposure, including the definition of new ones.

This study has the following limitations:

1. The breathing cycle of the people has not been considered while they are talking, i.e., inhalation has not been simulated, only exhalation (constant people's CO_2 emissions). No other situations have been considered such as people sneezing, coughing, singing, or laughing.
2. The following physical phenomena have been neglected: turbulent effects at the exiting air of people's mouths, solar loads, and radiative effects of people.
3. Regarding the turbulence treatment, an LES model would be more accurate than a URANS model. But this work focuses on the average behavior during the steady-state and compares the relative concentration between scenarios, for which the URANS models are suitable enough. In addition, considering the large number of scenarios analyzed here, the calculation time required for a LES model would be very high.
4. The elimination of infectious bioaerosols due to their viability loss, deposition on surfaces by gravitational and diffusional effects, and other mechanisms have been neglected. However, our assumptions are correct for small bioaerosols. They can be considered as a tracer gas [74].
5. It has not been considered the terrace as a dynamic environment, i.e., the effects of possible movements of people are not taken into account.
6. No experimental measurements have been carried out ex professor.

However, we think these limitations do not affect to main conclusions.

Author statement

E. Rivas: Conception and design of study, analysis and/or interpretation of data, Drafting the manuscript, Approval of the version of the manuscript to be published (the names of all authors must be listed), **J.L. Santiago:** Conception and design of study, analysis and/or interpretation of data, revising the manuscript critically for important intellectual content, Approval of the version of the manuscript to be published (the names of all authors must be listed), **F. Martin:** Conception and design of study, analysis and/or interpretation of data, revising the manuscript critically for important intellectual content, Approval of the version of the manuscript to be published (the names of all authors must be listed), **A. Martilli:** Conception and design of study, analysis and/or interpretation of data, revising the manuscript critically for important intellectual content, Approval of the version of the manuscript to be published (the names of all authors must be listed).

Declaration of competing interest

The authors declare that they have no known competing financial interests or personal relationships that could have appeared to influence the work reported in this paper.

Acknowledgements

References

[1] P. Kulkarni, P.A. Baron, K. Willeke, Aerosol Measurement: Principles, Techniques, and Applications, John Wiley & Sons, 2011, https://doi.org/10.1002/9781118001684.

[2] P. Baron, Generation and behavior of airborne particles (aerosols). https://www.cdc.gov/niosh/topics/aerosols/default.html, 2010.

[3] C. Chen, B. Zhao, Some questions on dispersion of human exhaled droplets in ventilation room: answers from numerical investigation, Indoor Air 20 (2010) 95–111, https://doi.org/10.1111/j.1600-0668.2009.00626.x.

[4] R.L. Riley, Airborne infection, Am. J. Med. 57 (1974) 466–475, https://doi.org/10.1016/0002-9343(74)90140-5.

[5] R. Tellier, Review of aerosol transmission of influenza a virus, Emerg. Infect. Dis. 12 (2006) 1657, https://doi.org/10.3201/eid1211.060426.

[6] I.T. Yu, Y. Li, T.W. Wong, W. Tam, A.T. Chan, J.H. Lee, D.Y. Leung, T. Ho, Evidence of airborne transmission of the severe acute respiratory syndrome virus, N. Engl. J. Med. 350 (2004) 1731–1739, https://doi.org/10.1056/nejmoa032867.

[7] R. Tellier, Y. Li, B.J. Cowling, J.W. Tang, Recognition of aerosol transmission of infectious agents: a commentary, BMC Infect. Dis. 19 (2019) 1–9, https://doi.org/10.1186/s12879-019-3707-y.

[8] K.A. Prather, L.C. Marr, R.T. Schooley, M.A. McDiarmid, M.E. Wilson, D.K. Milton, Airborne transmission of sars-cov-2, Science 370 (2020) 303–304, https://doi.org/10.1126/SCIENCE.ABF0521.

[9] T. Greenhalgh, J.L. Jimenez, K.A. Prather, Z. Tufekci, D. Fisman, R. Schooley, Ten scientific reasons in support of airborne transmission of sars-cov-2, Lancet 397 (2021) 1603–1605, https://doi.org/10.1016/S0140-6736(21)00869-2.

[10] European Communities/Eurostat, How Europeans Spend Their Time: Everyday Life of Women and Men: Data 1998-2002, Office for official publications of the European Communities, 2004. https://ec.europa.eu/eurostat/documents/3930297/5953614/KS-58-04-998-EN.PDF/c789a2ce-ed5b-4a0c-bcbf-693e699db7d7?version=1.0.

[11] T.C. Bulfone, M. Malekinejad, G.W. Rutherford, N. Razani, Outdoor transmission of sars-cov-2 and other respiratory viruses: a systematic review, J. Infect. Dis. 223 (2020) 550–561, https://doi.org/10.1093/infdis/jiaa742.

[12] CDC-Centers of Disease Control and Prevention, Scientific Brief: Sars-cov-2 Transmission, 2020. https://www.cdc.gov/coronavirus/2019-ncov/science/science-briefs/sars-cov-2-transmission.html#print.

[13] S. Asadi, A.S. Wexler, C.D. Cappa, S. Barreda, N.M. Bouvier, W.D. Ristenpart, Aerosol emission and superemission during human speech increase with voice loudness, Sci. Rep. 9 (2019) 1–10, https://doi.org/10.1038/s41598-019-38808-z.

[14] N.R. Jones, Z.U. Qureshi, R.J. Temple, J.P. Larwood, T. Greenhalgh, L. Bourouiba, Two metres or one: what is the evidence for physical distancing in covid-19? Br. Med. J. 370 (2020) https://doi.org/10.1136/bmj.m3223.

[15] World Health Organization, Roadmap to Improve and Ensure Good Indoor Ventilation in the Context of COVID-19, World Health Organization, 2021. https://www.who.int/publications/i/item/9789240021280.

[16] F. Memarzadeh, W. Xu, Role of air changes per hour (ach) in possible transmission of airborne infections, in: Building Simulation, Springer, 2012, pp. 15–28, https://doi.org/10.1007/s12273-011-0053-4.

[17] J. Pantelic, K.W. Tham, Adequacy of air change rate as the sole indicator of an air distribution system's effectiveness to mitigate airborne infectious disease transmission caused by a cough release in the room with overhead mixing ventilation: a case study, HVAC R Res. 19 (2013) 947–961, https://doi.org/10.1080/10789669.2013.842447.

[18] L. Morawska, J. Allen, W. Bahnfleth, P.M. Bluyssen, A. Boerstra, G. Buonanno, J. Cao, S.J. Dancer, A. Floto, F. Franchimon, et al., A paradigm shift to combat indoor respiratory infection, Science 372 (2021) 689–691, https://doi.org/10.1126/science.abg2025.

[19] Z.D. Bolashikov, A.K. Melikov, Methods for air cleaning and protection of building occupants from airborne pathogens, Build. Environ. 44 (2009) 1378–1385, https://doi.org/10.1016/j.buildenv.2008.09.001.

[20] J. Ren, Y. Wang, Q. Liu, Y. Liu, Numerical study of three ventilation strategies in a prefabricated covid-19 inpatient ward, Build. Environ. 188 (2021) 107467, https://doi.org/10.1016/j.buildenv.2020.107467.

[21] A. Hasan, Tracking the flu virus in a room mechanical ventilation using cfd tools and effective disinfection of an hvac system, Int. J. Air Cond. Refrig. 28 (2020) 2050019, https://doi.org/10.1142/S2010132520500194.

[22] J.M. Villafruela, I. Olmedo, F.A. Berlanga, M. Ruiz de Adana, Assessment of displacement ventilation systems in airborne infection risk in hospital rooms, PLoS One 14 (2019) e0211390, https://doi.org/10.1371/journal.pone.0211390.

[23] F. Berlanga, M.R. de Adana, I. Olmedo, J. Villafruela, J. San José, F. Castro, Experimental evaluation of thermal comfort, ventilation performance indices and exposure to airborne contaminant in an airborne infection isolation room equipped with a displacement air distribution system, Energy Build. 158 (2018) 209–221, https://doi.org/10.1016/j.enbuild.2017.09.100.

[24] M. VanSciver, S. Miller, J. Hertzberg, Particle image velocimetry of human cough, Aerosol. Sci. Technol. 45 (2011) 415–422, https://doi.org/10.1080/02786826.2010.542785.

[25] E. Riley, G. Murphy, R. Riley, Airborne spread of measles in a suburban elementary school, Am. J. Epidemiol. 107 (1978) 421–432.

[26] J. Jimenez, K. Human, K. Simpkins, Covid-19 Airborne Transmission Tool Available, 2020. https://cires.colorado.edu/news/covid-19-airborne-transmission-tool-available.

[27] K.R. Mead, A. Feng, D.R. Hammond, S.A. Shulman, Expedient Methods for Surge Airborne Isolation within Healthcare Settings during Response to a Natural or Manmade Epidemic: in-depth Report, 2012. https://www.cdc.gov/niosh/surveyreports/pdfs/301-05f.pdf.

[28] S. Peng, Q. Chen, E. Liu, The Role of Computational Fluid Dynamics Tools on Investigation of Pathogen Transmission: Prevention and Control, Science of The Total Environment, 2020, p. 142090, https://doi.org/10.1016/j.scitotenv.2020.142090.

[29] G. Buonanno, L. Stabile, L. Morawska, Estimation of airborne viral emission: quanta emission rate of sars-cov-2 for infection risk assessment, Environ. Int. 141 (2020) 105794, https://doi.org/10.1016/j.envint.2020.105794.

[30] V. Vuorinen, M. Aarnio, M. Alava, V. Alopaeus, N. Atanasova, M. Auvinen, N. Balasubramanian, H. Bordbar, P. Erästö, R. Grande, N. Hayward, A. Hellsten, S. Hostikka, J. Hokkanen, O. Kaario, A. Karvinen, I. Kivistö, M. Korhonen, R. Kosonen, J. Kuusela, S. Lestinen, E. Laurila, H.J. Nieminen, P. Peltonen, J. Pokki, A. Puisto, P. Råback, H. Salmenjoki, T. Sironen, M. Österberg, Modelling aerosol transport and virus exposure with numerical simulations in relation to sars-cov-2 transmission by inhalation indoors, Saf. Sci. 130 (2020) 104866, https://doi.org/10.1016/j.ssci.2020.104866.

[31] Y. Li, H. Qian, J. Hang, X. Chen, P. Cheng, H. Ling, S. Wang, P. Liang, J. Li, S. Xiao, et al., Probable airborne transmission of sars-cov-2 in a poorly ventilated restaurant, Build. Environ. 196 (2021) 107788, https://doi.org/10.1016/j.buildenv.2021.107788.

[32] L. Borro, L. Mazzei, M. Raponi, P. Piscitelli, A. Miani, A. Secinaro, The role of air conditioning in the diffusion of sars-cov-2 in indoor environments: a first computational fluid dynamic model, based on investigations performed at the vatican state children's hospital, Environ. Res. 193 (2021) 110343, https://doi.org/10.1016/j.envres.2020.110343.

[33] A. Foster, M. Kinzel, Estimating covid-19 exposure in a classroom setting: a comparison between mathematical and numerical models, Phys. Fluids 33 (2021), 021904, https://doi.org/10.1063/5.0040755.

[34] C. Liang, S. Jiang, X. Shao, H. Wang, S. Yan, Z. Yang, X. Li, Is it safe to reopen theaters during the covid-19 pandemic? Front. Built Environ. 7 (2021) 12.

[35] T. Dbouk, D. Drikakis, On coughing and airborne droplet transmission to humans, Phys. Fluids 32 (2020), 053310, https://doi.org/10.1063/5.0011960.

[36] S. Rudnick, D. Milton, Risk of indoor airborne infection transmission estimated from carbon dioxide concentration, Indoor Air 13 (2003) 237–245.

[37] S.J. Emmerich, A.K. Persily, State-of-the-Art Review of CO_2 Demand Controlled Ventilation Technology and Application, NIST Interagency/Internal Report (NISTIR), National Institute of Standards and Technology, Gaithersburg, MD, 2001, https://tsapps.nist.gov/publication/get_pdf.cfm?pub_id=860846.

[38] C.M. Issarow, N. Mulder, R. Wood, Modelling the risk of airborne infectious disease using exhaled air, J. Theor. Biol. 372 (2015) 100–106, https://doi.org/10.1016/j.jtbi.2015.02.010.

[39] Z. Peng, J.L. Jimenez, Exhaled co2 as a covid-19 infection risk proxy for different indoor environments and activities, Environ. Sci. Technol. Lett. 8 (2021) 392–397, https://doi.org/10.1021/acs.estlett.1c00183.

[40] N. Gao, J. Niu, Modeling particle dispersion and deposition in indoor environments, Atmos. Environ. 41 (2007) 3862–3876, https://doi.org/10.1016/j.atmosenv.2007.01.016.

[41] Q. He, J. Niu, N. Gao, T. Zhu, J. Wu, CFD study of exhaled droplet transmission between occupants under different ventilation strategies in a typical office room, Build. Environ. 46 (2011) 397–408, https://doi.org/10.1016/j.buildenv.2010.08.003.

[42] W. Schade, V. Reimer, M. Seipenbusch, U. Willer, Experimental investigation of aerosol and co2 dispersion for evaluation of covid-19 infection risk in a concert hall, Int. J. Environ. Res. Publ. Health 18 (2021) 3037, https://doi.org/10.3390/ijerph18063037.

[43] T.R. Sosnowski, Inhaled aerosols: their role in covid-19 transmission, including biophysical interactions in the lungs, Curr. Opin. Colloid Interface Sci. 54 (2021) 101451, https://doi.org/10.1016/j.cocis.2021.101451.

[44] Ayuntamiento de Madrid, Ordenanza de terrazas y quioscos de hostelería y restauración - gestiones y trámites, 2013. https://sede.madrid.es/portal/site/tramites/menuitem.5dd4485239c96e10f7a72106a8a409a0/?vgnextoid=6c30a49604150410VgnVCM1000000b205a0aRCRD&vgnextchannel=e81965dd72ede410VgnVCM1000000b205a0aRCRD.

[45] J. Franke, A. Hellsten, H. Schlünzen, B. Carissimo, Best Practice Guideline for the CFD Simulation of Flows in the Urban Environment: COST Action 732 Quality Assurance and Improvement of Microscale Meteorological Models, Meteorological Institute-University of Hamburg, 2007. https://mi-pub.cen.uni-hamburg.de/fileadmin/files/forschung/techmet/cost/cost_732/pdf/BestPractiseGuideline_1-5-2007-www.pdf.

[46] 3D CAD Browser, Country Restaurant Free 3D Model, 2020. https://www.3dcadbrowser.com/3d-model/country-restaurant.

[47] StrataSYS, GrabCAD: free CAD Files, 2021. https://grabcad.com/.

[48] Siemens Digital Industries Software, Sim Center STAR-CCM+, 2021. https://www.plm.automation.siemens.com/global/es/products/simcenter/STAR-CCM.html.

[49] H. Zhang, D. Li, L. Xie, Y. Xiao, Documentary research of human respiratory droplet characteristics, Procedia Eng. 121 (2015) 1365–1374, https://doi.org/10.1016/j.proeng.2015.09.023.

[50] D. Spalding, Concentration fluctuations in a round turbulent free jet, Chem. Eng. Sci. 26 (1971) 95–107, https://doi.org/10.1016/0009-2509(71)86083-9.

[51] Y. Li, T. Stathopoulos, Numerical evaluation of wind-induced dispersion of pollutants around a building, J. Wind Eng. Ind. Aerod. 67 (1997) 757–766, https://doi.org/10.1016/S0167-6105(97)00116-5.

[52] X. Wang, K.F. McNamara, Evaluation of cfd simulation using rans turbulence models for building effects on pollutant dispersion, Environ. Fluid Mech. 6 (2006) 181–202, https://doi.org/10.1007/s10652-005-5656-9.

[53] P. Richards, R. Hoxey, Appropriate boundary conditions for computational wind engineering models using the $\kappa - \varepsilon$ turbulence model, J. Wind Eng. Ind. Aerod. 46 (1993) 145–153, https://doi.org/10.1016/0167-6105(93)90124-7.

[54] Agencia Estatal de Meteorología - AEMET, Gobierno de España, Madrid aeropuerto, 2021. http://www.aemet.es/es/serviciosclimaticos/datosclimatologicos/valoresclimatologicos?l=3129&k=28.

[55] American Society of Heating, Refrigerating and Air-Conditioning Engineers, 2017 ASHRAE Handbook: Fundamentals, ASHRAE, Atlanta, GA, 2017.

[56] B.E. Ainsworth, W.L. Haskell, A.S. Leon, D.R. Jacobs Jr., H.J. Montoye, J.F. Sallis, R.S. Paffenbarger Jr., Compendium of physical activities: classification of energy costs of human physical activities, Med. Sci. Sports Exerc. 25 (1993) 71–80, https://doi.org/10.1249/00005768-199301000-00011.

[57] R. Mosteller, Simplified calculation of body-surface area, N. Engl. J. Med. 317 (1987), https://doi.org/10.1056/nejm198710223171717, 1098–1098.

[58] L. Davis, Body Physics: Motion to Metabolism. Open Oregon Educational Resources, 2019. https://openoregon.pressbooks.pub/bodyphysics/.

[59] E. Rivas, J.L. Santiago, Y. Lechón, F. Martín, A. Ariño, J.J. Pons, J.M. Santamaría, Cfd modelling of air quality in pamplona city (Spain): assessment, stations spatial representativeness and health impacts valuation, Sci. Total Environ. 649 (2019) 1362–1380, https://doi.org/10.1016/j.scitotenv.2018.08.315.

[60] J.L. Santiago, R. Buccolieri, E. Rivas, H. Calvete-Sogo, B. Sanchez, A. Martilli, R. Alonso, D. Elustondo, J.M. Santamaria, F. Martin, Cfd modelling of vegetation barrier effects on the reduction of traffic-related pollutant concentration in an avenue of pamplona, Spain, Sustain. Cities Soc. 48 (2019), 101559.

[61] H.D. Goodfellow, E. Tahti, Industrial Ventilation Design Guidebook, Academic press, 2001, https://doi.org/10.1016/b978-0-12-289676-7.x5000-0.

[62] B. Blocken, F. Malizia, T. van Druenen, T. Marchal, Towards aerodynamically equivalent covid19 1.5 m social distancing for walking and running, Urban Phys. (2020). Preprint, http://www.urbanphysics.net/Social%20Distancing%20v20_White_Paper.pdf.

[63] Q. Zhou, H. Qian, L. Liu, Numerical investigation of airborne infection in naturally ventilated hospital wards with central-corridor type, Indoor Built Environ. 27 (2018) 59–69, https://doi.org/10.1177/1420326X16667177.

[64] B. Chenari, J. Dias Carrilho, M. Gameiro da Silva, Towards sustainable, energy-efficient and healthy ventilation strategies in buildings: a review, Renew. Sustain. Energy Rev. 59 (2016) 1426–1447, https://doi.org/10.1016/j.rser.2016.01.074.

[65] N. Khan, Y. Su, S.B. Riffat, A review on wind driven ventilation techniques, Energy Build. 40 (2008) 1586–1604, https://doi.org/10.1016/j.enbuild.2008.02.015.

[66] H. Nishiura, H. Oshitani, T. Kobayashi, T. Saito, T. Sunagawa, T. Matsui, T. Wakita, M. COVID, R. Team, M. Suzuki, Closed environments facilitate secondary transmission of coronavirus disease 2019 (covid-19), MedRxiv (2020), https://doi.org/10.1101/2020.02.28.20029272.

[67] Z.D. Guo, Z.Y. Wang, S.F. Zhang, X. Li, L. Li, C. Li, Y. Cui, R.B. Fu, Y.Z. Dong, X.Y. Chi, et al., Aerosol and surface distribution of severe acute respiratory syndrome coronavirus 2 in hospital wards, wuhan, China, 2020, Emerg. Infect. Dis. 26 (2020) 1586, https://doi.org/10.3201/eid2607.200885.

[68] J.M. Villafruela, F. Castro, J.F. San José, J. Saint-Martin, Comparison of air change efficiency, contaminant removal effectiveness and infection risk as iaq indices in isolation rooms, Energy Build. 57 (2013) 210–219, https://doi.org/10.1016/j.enbuild.2012.10.053.

[69] K.C. Chung, S.P. Hsu, Effect of ventilation pattern on room air and contaminant distribution, Build. Environ. 36 (2001) 989–998, https://doi.org/10.1016/S0360-1323(00)00051-2.

[70] E.T. Richardson, C.D. Morrow, D.B. Kalil, S. Ginsberg, L.G. Bekker, Correction: Shared Air: A Renewed Focus on Ventilation for the Prevention of Tuberculosis Transmission, 2014, https://doi.org/10.1371/journal.pone.0106216.

[71] A. Rizk, M. El Morsi, M. Elwan, A review on wind-driven cross–ventilation techniques inside single rooms, Int. J. Sci. Eng. Res. 6 (2018) 75.

[72] J. Lu, J. Gu, J. Gu, K. Li, C. Xu, W. Su, Z. Lai, D. Zhou, C. Yu, B. Xu, Z. Yang, Covid-19 outbreak associated with air conditioning in restaurant, guangzhou, China, 2020, Emerg. Infect. Dis. 26 (2020) 1628–1631, https://doi.org/10.3201/eid2607.200764.

[73] S.L. Miller, W.W. Nazaroff, J.L. Jimenez, A. Boerstra, G. Buonanno, S.J. Dancer, J. Kurnitski, L.C. Marr, L. Morawska, C. Noakes, Transmission of sars-cov-2 by inhalation of respiratory aerosol in the skagit valley chorale superspreading event, Indoor Air 31 (2021) 314–323, https://doi.org/10.1111/ina.12751.

[74] E. Hathway, C. Noakes, P. Sleigh, L. Fletcher, Cfd simulation of airborne pathogen transport due to human activities, Build. Environ. 46 (2011) 2500–2511, https://doi.org/10.1016/j.buildenv.2011.06.001.

Nomenclature

Acronyms
ACH: Air Change per Hour
AQMS: Air Quality Monitoring Station
BC: Black Carbon
CDC: Center for Disease Control and Prevention
CFD: Computational Fluid Dynamics
CFL: Courant number
CLO: Clothing insulation
DV: Displacement Ventilation
EC: European Commission
ICU: Intensive Care Unit
LES: Large Eddy Simulations
MERS: Middle East Respiratory Syndrome
MET: Metabolic rate
MV: Mixing Ventilation
PIV: Particle Image Velocimetry
R_0: Reproductive Number
SARS − COV: Severe Acute Respiratory Syndrome Coronavirus
UFAD: Under-floor Air Distribution
URANS: Unsteady Reynolds-Averaged Navier-Stokes
WHO: World Health Organization

Subscripts
0: Initial
D: Down
I: Intermediate
in: Inlet
N: North
out: Outlet
U: Up
W: West

Symbols
(x, y, z): Cartesian coordinates (m)
ΔS: Surface size (m^2)
Δt: Time-step (s)
ΔV: Volume size (m^3)
ṁ: Mass flow rate (kg·s^{-1})
ε: Turbulent dissipation rate
κ: Turbulent kinetic energy (J·kg^{-1})
τ: Characteristic time (s)
$\vec{r}$: Position (m)
C: Concentration (ppm)
H: Height (m)
S: Surface (m^2)
T: Temperature (°C)
t: Time (s)
u: Velocity (m·s^{-1})
V: Volume (m^3)